(18). In this study, we analyzed in vivo infection of a popular picornavirus, PV, using PVR transgenic (PVRtg) mice, which show a neurotropic phenotype during PV infection similar to humans (19, 20). Using this mouse model, in combination with TICAM-1$^{-/-}$ or IPS-1$^{-/-}$ mice, we present evidence that the host TICAM-1 pathway, particularly in macrophages (Mf), serves as a source of type I IFN induction and protects host PVRtg mice from PV infection and paralytic death. Thus, the strategy for host protection against picornaviruses is not simply based on the MDA5-dependent dsRNA recognition, but is variable depending on picornavirus species.

Materials and Methods

Mice

All mice were backcrossed with C57BL/6 mice more than seven times before use. TICAM-1$^{-/-}$ (21) and IPS-1$^{-/-}$ mice (this study) were generated in our laboratory. TLR3$^{-/-}$ (4), IRF-3$^{-/-}$, and IRF-7$^{-/-}$ mice (22) were provided by Drs. S. Akira (Osaka University, Osaka, Japan) and T. Taniguchi (University of Tokyo, Tokyo, Japan). PVRtg mice were provided as reported previously (20). All mice were maintained under specific pathogen-free conditions in the Animal Facility at Hokkaido University Graduate School of Medicine (Sapporo, Japan). Animal experiments were performed according to the guidelines set by the Animal Safety Center, Japan.

Generation of IPS-1–deficient mice

The *IPS-1* gene was amplified by PCR using genomic DNA extracted from embryonic stem cells. The targeting vector was constructed by replacing the second and third exons with a neomycin-resistance gene cassette (Neo), and an HSV thymidine kinase driven by the PGK promoter was inserted into the genomic fragment for negative selection. After the targeting vector was transfected into 129/Sv mice-derived embryonic stem cells, G418 and ganciclovir doubly resistant colonies were selected and screened by PCR. The targeted cell line was injected into C57BL/6 blastocysts, resulting in the birth of male chimeric mice. These mice were then backcrossed with C57BL/6 mice. The disruption of the *IPS-1* gene was confirmed by PCR for the long and short arms. The abolishment of IPS-1 mRNA expression was confirmed by real-time quantitative PCR (RT-qPCR).

Cells, viruses, and reagents

Wild-type (WT) and TICAM-1$^{-/-}$ mouse embryonic fibroblasts (MEF) were prepared from 12.5- to 13.5-d-old embryos. PV, strain Mahoney, was amplified in Vero cells, and the viral titer was determined by a plaque assay. Bone marrow (BM) cells were prepared from the femur and tibia. The cells were cultured in RPMI 1640 (Invitrogen, New York, NY) supplemented with 10% FCS, 100 μM 2-ME, and 10 ng/ml murine GM-CSF or the culture supernatant of NIH3T3 cells expressing M-CSF. After 6 d, cells were collected and used as bone marrow-derived dendritic cells (BM-DC) or BM-derived macrophages (BM-Mf). For the preparation of BM-DC and BM-Mf, the medium was changed every 2 d. Splenic DC and NK cells were isolated using the MACS system (Miltenyi Biotec, Auburn, CA).

Experimental infection of mice

Five- to 8-wk-old C57BL/6 female mice were used throughout this study. Mice of different genotypes were i.p. or i.v. infected with PV at the doses indicated. The viability of the infected mice was monitored for 2 wk. We collected sera from the mice at different time points to measure viral titers by a plaque assay and cytokine levels by an ELISA. To determine the tissue viral titer, mice were euthanized and organs were aseptically removed and frozen by liquid nitrogen. Because the organs were not perfused before organs were removed, virus titers were determined including blood. Specimens were homogenized in 2 ml PBS on ice, and titers were determined by a plaque assay.

ELISA

Culture supernatants of cells (10^5) seeded on 24-well plates or sera were collected and analyzed for cytokine levels with ELISA. ELISA kits for IFN-α and IFN-β were purchased from PBL Biomedical Laboratories. ELISA was performed according to the manufacturer's instructions.

qPCR

For qPCR, total RNA was extracted with TRIzol (Invitrogen), and 0.2–0.5 μg RNA was reverse-transcribed using a high-capacity cDNA transcription kit (Applied Biosystems, Piscataway, NJ) with random primers according to the manufacturer's instructions. qPCR was performed using a Step One real-time PCR system (Applied Biosystems).

In vivo blocking of NK activity

Mice (PVRtg and PVRtg/TICAM-1$^{-/-}$) were i.p. injected with 250 μg anti-NK1.1 Ab, asialoGM1 Ab, or control PBS as described previously (21). One day later, the mice were i.p. inoculated with 10^4 PFU PV. One to 7 d after PV injection, depletion of peripheral NK1.1$^+$ cells was confirmed by flow cytometry. Then, the mortality of the mice was monitored. In some experiments, the spleen cells were harvested and NK cells (DX5$^+$ cells) were positively isolated using the MACS system (Miltenyi Biotec). The DX5$^+$ NK cells were suspended in RPMI 1640 containing 10% FCS and mixed with ^{51}Cr-labeled B16D8 cells at the indicated E:T ratios. After 4 h, the supernatants were harvested and [^{51}Cr] release was measured.

Statistical analysis

Statistical significance of differences between groups was determined by the Student *t* test, and survival curves were analyzed by the log-rank test using Prism 4 for Macintosh software (GraphPad Software). Student *t* tests and χ^2 goodness-of-fit tests were performed using Microsoft Excel software and a χ^2 distribution table.

Results

TICAM-1 is essential for protection of PVRtg mice against PV infection

Mice lacking the *mda-5* gene abrogate the production of type I IFN in response to EMCV infection and are more susceptible to infection with EMCV (13, 17). Because EMCV is a picornavirus, it has been proposed that MDA5 is critical for sensing picornavirus infection. In infected cells, picornaviruses efficiently generate long dsRNA, which is recognized by the cytoplasmic dsRNA sensor MDA5 (23). The 5′ end of the PV genomic RNA is linked to a VPg protein (16), not to a 5′-triphosphate, a major ligand for another cytoplasmic RNA sensor, RIG-I (24, 25). Thus, we first tested, using the PVRtg mouse model (20), whether the mortality of PV-infected mice is affected by disruption of IPS-1 (Fig. 1*A*). Approximately 70% of WT (PVRtg) mice and ~40% of IPS-1$^{-/-}$ mice survived >10 d postinoculation at an i.p. dose of 2×10^4 PFU. No statistical significance between these two groups was detected (Fig. 1*A*). In the same experiments, TICAM-1$^{-/-}$ mice died within 5 d by paralysis (Fig. 1*B*).

We next investigated the effect of the route of PV infection on mortality in this mouse model. PV (2×10^3 PFU) was injected i.p. or i.v. into WT and TICAM-1 mice and their mortality was examined (Fig. 1*C*, 1*D*). All TICAM-1$^{-/-}$ mice died by paralysis within 7.5 d irrespective of the injection route. The significance of this early mortality rate of PV-infected TICAM-1$^{-/-}$ mice was supported by statistical analysis. The mortality rates were slightly high in WT mice compared with IPS-1$^{-/-}$ mice when PV loads in mice were not very high (Supplemental Fig. 1*A*). This tendency seemingly diminished by early death of IPS-1$^{-/-}$ mice with high doses of PV input. These data suggested that TICAM-1, rather than IPS-1 (or the sensors RIG-I and MDA5), is a critical factor in protecting mice from PV-mediated paralytic death. This conclusion was confirmed using RIG-I$^{-/-}$ and MDA5$^{-/-}$ mice with a PVRtg background (S. Abe, K. Fujii, and S. Koike, submitted for publication).

These results showed a discrepancy with previous indications that MDA5 is critical in picornavirus protection (13). We therefore tested the dose dependence of PV in the survival of WT versus TICAM-1$^{-/-}$ mice. Surprisingly, high doses of PV (2×10^5 and 2×10^6 PFU) induced paralytic death in all WT as well as TICAM-1$^{-/-}$ mice within 6 d (Fig. 2*A*, 2*B*). Thus, high doses of PV (>2×10^5 PFU) appear to overpower the TICAM-1 PV-protective activity in vivo, which confirmed previous findings using other picornaviruses (13). TICAM-1 was most effective in

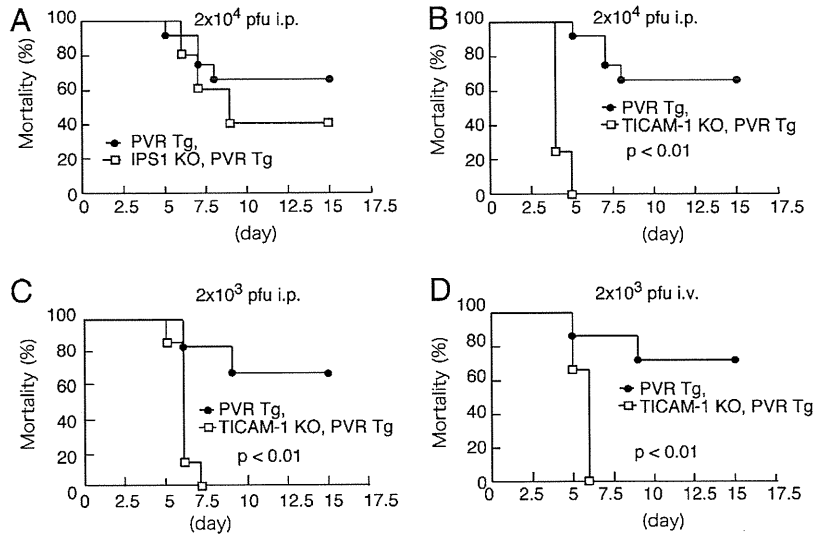

FIGURE 1. Survival of WT, TICAM-1 KO, and IPS-1 KO mice following i.p. or i.v. PV infection. *A* and *B*, PV (2×10^4 PFU) was infected via the i.p. route into WT and IPS-1 (*A*) or TICAM-1 (*B*) KO mice ($n \geq 5$), and survival was monitored for 14 d. *C* and *D*, PV (2×10^3 PFU) was infected via the i.p. (*C*) or i.v. (*D*) route into WT and TICAM-1 KO mice ($n \geq 5$), and survival was monitored for 14 d.

the survival against PV infection at low dose ($<2 \times 10^4$ PFU) (Figs. 1*B*, 1*C*, 2*C*). Similar results were obtained with the PV infection study (S. Abe, K. Fujii, and S. Koike, submitted for publication) when TICAM-$1^{-/-}$ mice were substituted with TLR$3^{-/-}$ or IRF-3/7 double-knockout (KO) mice. Results were confirmed using IRF-$3^{-/-}$ and IRF-$7^{-/-}$ mice (26). These results are essentially consistent with previous reports using a PVRtg/IFNAR$^{-/-}$ mouse model (27), in which type I IFN is critical for PV permissiveness, particularly in the intestine of PVRtg mice.

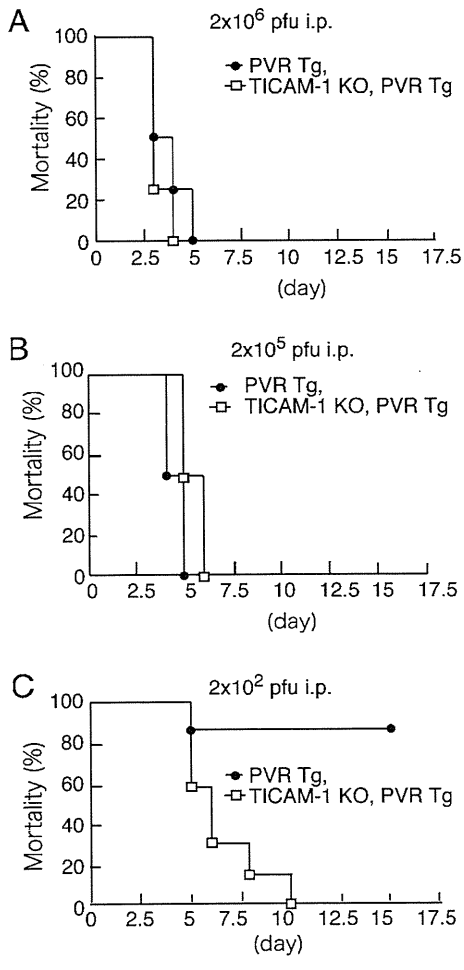

FIGURE 2. High doses of PV disable the protective effect of TICAM-1. WT and TICAM-1 KO mice ($n \geq 6$) were i.p. infected with 2×10^6 (*A*), 2×10^5 (*B*), or 2×10^2 PFU (*C*) PV and survival was monitored for 14 d.

TICAM-1–dependent type I IFN induction in PVRtg mice

PV titers in various organs were measured with WT and TICAM-$1^{-/-}$ mice i.p. injected with 2×10^4 PFU PV. In most organs, PV titers were higher in TICAM-$1^{-/-}$ mice than in WT mice at day 3 post-infection (Fig. 3*A*). The PV titer ratio in TICAM-$1^{-/-}$ versus WT mice was also high in the lung (Fig. 3*A*). In most organs except for the large intestine, high PV titers were harvested in TICAM-$1^{-/-}$ mice compared with WT mice. The difference in local PV titers between WT and TICAM-$1^{-/-}$ mice was culminated in the lung and spinal cord (Fig. 3*A*). Serum PV titers were increased within 48 h

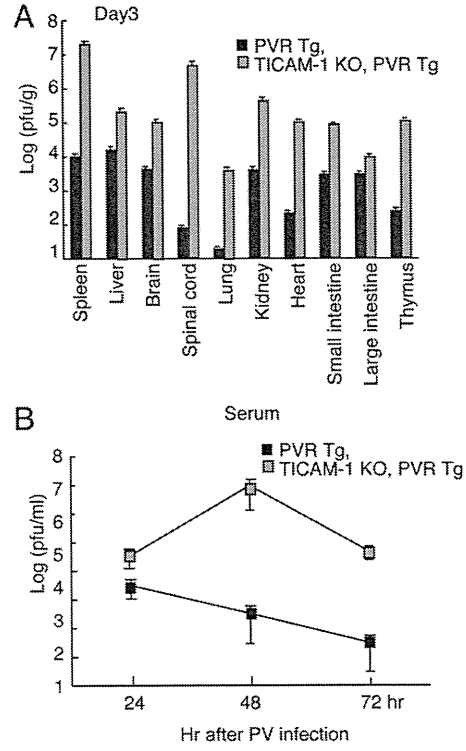

FIGURE 3. Viral titers in organs and serum following PV infection. WT and TICAM-1 KO mice were infected i.p. with 2×10^4 PFU PV. The viral titers in each organ (*A*) and sera (*B*) were measured by a plaque assay. Data are shown as means ± SD of three independent samples.

after PV i.p. injection in TICAM-1$^{-/-}$ mice compared with WT mice (Fig. 3*B*).

IFN-α/β levels were measured with sera from WT, IPS-1$^{-/-}$, and TICAM-1$^{-/-}$ mice, but they were barely detected in these PV-infected mice (Supplemental Fig. 1*B*). Only i.v. injection of high PV titers (an example shows $>4 \times 10^6$ PFU) allowed WT mice to release type I IFN within 12 h (Supplemental Fig. 1*B*). No IFN was detected in blood in TICAM-1$^{-/-}$ and IPS-1$^{-/-}$ mice even in this high-dose setting. However, IFN-α production was reproduced in a cell type level (peritoneal Mf) in vitro (Supplemental Fig. 1*C*). PV infection-mediated cell death (28) and degradation of MDA5 protein (29) may be major causes for this undetectable type I IFN production during in vivo PV infection.

TICAM-1 pathway contributes to IFN-β induction in WT mice with low PV titers

We next determined the mRNA levels of type I IFN in each organ extracted from PV (2×10^4 PFU)-infected WT and TICAM-1$^{-/-}$ mice. IFN-β mRNA was upregulated in all of the organs tested in WT mice within 12 h in response to PV injection (i.p.) (Fig. 4*A*). In contrast, only a low increase in IFN-β mRNA was detected in the organs of TICAM-1$^{-/-}$ mice (Fig. 4*A*). IFN-α2 mRNA was upregulated in the organs of TICAM-1$^{-/-}$ and WT mice to similar extents in response to PV injection (2×10^4 PFU, i.p.) (Fig. 4*B*). Notable decreases in IFN-α2 mRNA were observed in the TICAM-1$^{-/-}$ spleen and spinal cord compared with WT controls (Fig. 4*B*). The mRNA levels of genes associated with type I IFN induction were evaluated by qPCR, and no unique differences were observed between the splenocytes from PV-injected TICAM-1$^{-/-}$ and IPS-1$^{-/-}$ mice (Supplemental Fig. 1*D*). Hence, type I IFN mRNA is generally upregulated via TICAM-1 in the local organs of PVRtg WT mice during PV infection.

The mRNA levels of IFN-inducible genes and other cytokines were determined in spleen cells after PV infection. IFN-λ and IFN-γ–induced protein 10 (IP-10) mRNA were upregulated in the spleen cells of WT, but not TICAM-1$^{-/-}$ mice, after PV infection (multiplicity of infection [MOI] of 1) (Fig. 4*C*), with profiles similar to that of IFN-β mRNA (Fig. 4*C*). A sensor for 5′-triphosphorylated RNA, IFN-induced protein with tetratripeptide repeats 1 (IFIT-1), was also upregulated through PV infection (Fig. 4*C*). TNF-α, IL-10, IL-12p40, and IFN-γ, which may be associated with infectious cell death, were barely upregulated in spleen cells in response to PV infection (Supplemental Fig. 1*E*).

TICAM-1–dependent type I IFN induction by PV depends on Mf in PVRtg mice

The types of cells that participate in type I IFN induction in the spleen were examined by sorting spleen cells. IFN-β and IFN-α2 were found to be induced in WT CD11c$^+$ DC (Fig. 5*A*), whereas CD11c$^-$ cells barely induced type I IFN. Furthermore, IFN-β and IFN-α2 were barely induced in TICAM-1$^{-/-}$ CD11c$^+$ cells (Fig. 5*B*). Participation of IPS-1 in type I IFN induction in CD11c$^+$ myeloid cells is less compared with that of TICAM-1 (Fig. 5*B*).

Splenic CD8α$^+$CD11c$^+$ and CD4$^+$CD11c$^+$ cells were separated by MACS beads and their response to PV (MOI of 1) was analyzed by determining the mRNA levels of type I IFN (Fig. 5*C*). CD8α$^+$CD11c$^+$ cells, but not the CD4$^+$CD11c$^+$ cells, of WT mice were responsible for type I IFN induction by PV. There was a CD4$^-$CD8α$^-$ population of DC in the spleen and this type of cells did not induce type I IFN in response to PV (Supplemental Fig. 2). The generation of the mRNA of type I IFN and IFIT-1 by PV infection was abrogated in the TICAM-1$^{-/-}$ CD8α$^+$CD11c$^+$ splenic DC (Fig. 5*D*). Also, CD4/8α double-negative DC failed to express type I IFNs (Supplemental Fig. 2). Thus, CD8α$^+$CD11c$^+$ DC, which reportedly express TLR3 (30), are the source of type I IFN in PV-infected PVRtg mice.

We finally confirmed that type I IFN is locally induced in TLR3$^+$ myeloid cells during PV infection. BM-Mf and BM-DC were prepared from mouse BM and challenged with PV (MOI of 1). These cells express TLR3 in the endosome as previously reported about mouse BM-DC (30) and human monocyte-derived DC (31). BM-Mf showed similar profiles of type I IFN mRNA to those of PV-infected splenocytes (Figs. 4*C*, 6*A*). However, IFN-λ and IP-10 mRNA were not detectable in PV-infected BM-Mf, the reason for which remains unclear (Fig. 6*A*). IL-12p40, a representative TICAM-1–dependent gene, was transiently upregulated

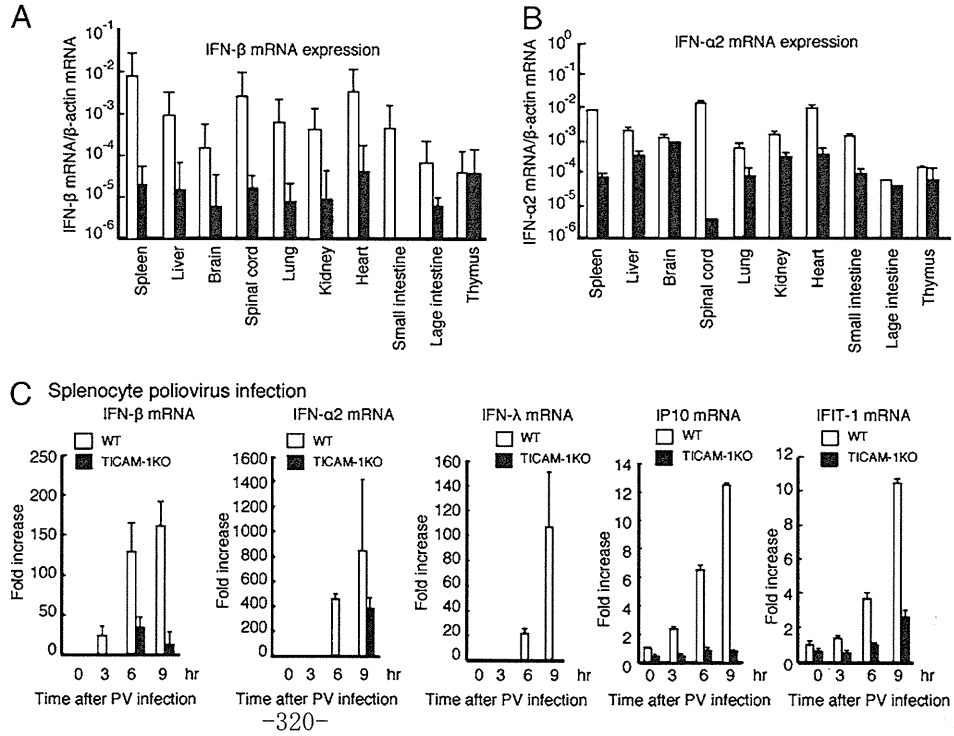

FIGURE 4. The expression of type I IFN following PV infection. *A* and *B*, WT and TICAM-1 KO mice were infected i.p. with 2×10^4 PFU PV. Three days postinfection, the mRNA expression levels of IFN-β (*A*) and IFN-α (*B*, *C*) were determined by RT-qPCR. *C*, Splenocytes (5×10^5) were infected with PV (MOI of 1) and the mRNA expression levels of IFN-β, IFN-α2, IFN-λ, IP-10, and IFIT-1 were measured by RT-qPCR. Data are shown as means ± SD and are representative of three independent experiments.

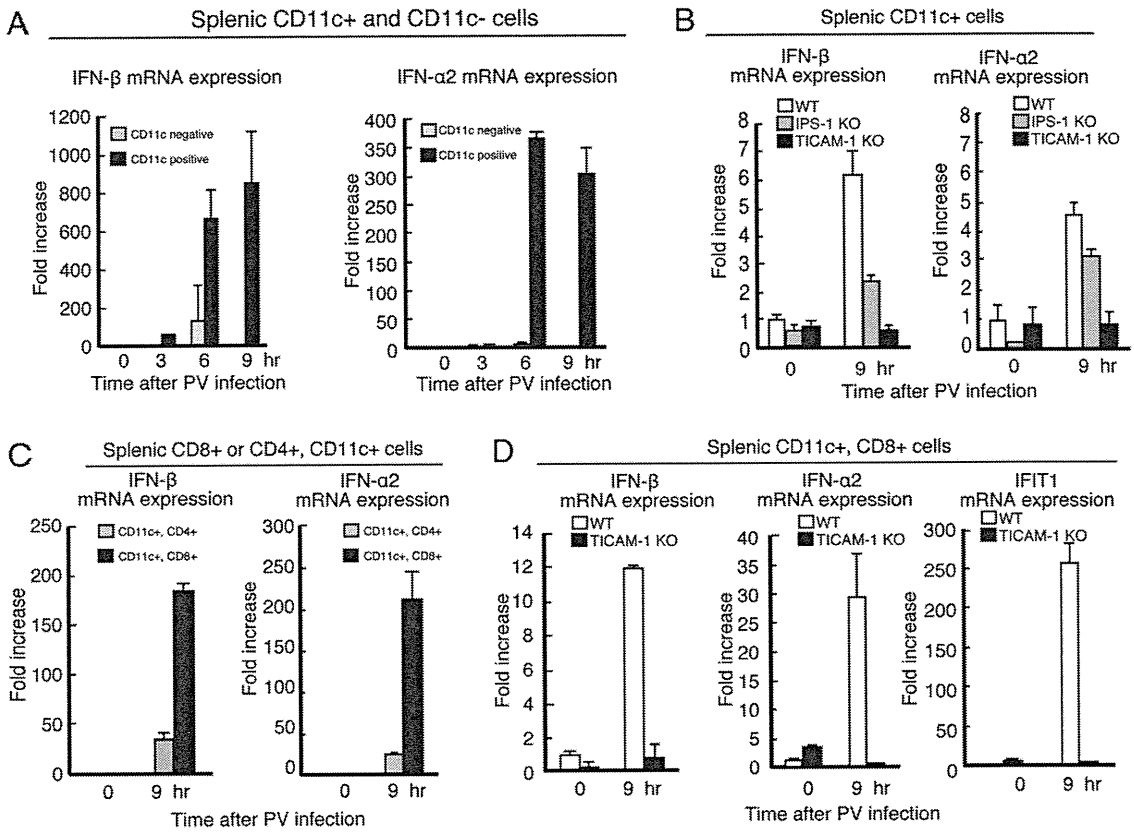

FIGURE 5. The expression of type I IFN in splenic DC. *A*, were isolated from WT spleens using the MACS system. $CD11c^+$ or $CD11c^-$ cells (5×10^5) were infected with PV (MOI of 1), and the mRNA expression of type I IFNs was measured by RT-qPCR. *B*, WT, TICAM-1, and IPS-1 knockout splenic $CD11c^+$ cells were infected with PV, and the expression of type I IFNs was measured by RT-qPCR. *C*, $CD8\alpha^+CD11c^+$ cells and $CD4^+CD11c^+$ cells were isolated from WT spleens and infected with PV (MOI of 1). The expression of type I IFNs was measured by RT-qPCR. *D*, $CD8\alpha^+CD11c^+$ splenic cells were isolated from WT and TICAM-1 KO mice and infected with PV (MOI of 1). The expressions of type I IFNs and IFIT-1 were measured by RT-qPCR. Data are shown as means ± SD and are representative of three independent experiments.

in BM-Mf ~4 h after PV infection (Supplemental Fig. 3). Similarly, but less prominently, the profiles of type I IFN and IL-12p40 were observed in BM-DC (Fig. 6*A*, Supplemental Fig. 3) and $CD11c^+CD8^+$ splenic DC (Fig. 5*D*). Therefore, taken together, these results indicate that IL-12 and IFN-α/β are only minimally upregulated in splenic DC in a PV-dependent manner.

The production of IFN-α was determined by ELISA in the supernatant of PV-infected BM-Mf and BM-DC (Fig. 6*C*). BM-Mf prepared from WT mice generated higher amounts of IFN-α than did those from TICAM-$1^{-/-}$ mice. Although similar results were obtained with BM-DC, the effect of TICAM-1 depletion was not statistically significant (Fig. 6*C*).

NK cells and MEF do not play major roles in protection against PV infection

Using NK1.1-depleted mice, we tested the possible participation of NK cells in the protection of PVRtg mice from PV infection (Fig. 7). $NK1.1^+$ cells were depleted from mouse blood 1 d after injection (i.p.) of NK1.1 Ab into WT (Fig. 7*A*) and TICAM-$1^{-/-}$ mice. After PV challenge, WT mice inoculated with control saline and NK1.1 Ab survived similarly, whereas TICAM-$1^{-/-}$ mice were all killed by PV within 7.5 d irrespective of NK1.1 pretreatment (Fig. 7*B*). Hence, NK cell activation does not affect PV-derived death. The lack of TICAM-1 was also found to have no effect on the NK cell-mediated rescue of PV-infected mice.

Mouse fibroblasts are known to be a potential source of type I IFN (13). We therefore checked whether MEF induce type I IFN and protection against PV (Supplemental Fig. 4). MEF from WT PVRtg mice were susceptible to PV, with cell death being observed at an MOI of 1. MEF from TICAM-$1^{-/-}$ PVRtg mice were 1 log more susceptible to PV, with cell death occurring at an MOI of 0.1 (Supplemental Fig. 4*A*). IFN-β was upregulated in PV-infected MEF to only a slightly higher level in PVRtg MEF than in TICAM-$1^{-/-}$ PVRtg MEF (Supplemental Fig. 4*B*). These results suggested that the large difference in the PV survival rate between WT and TICAM-$1^{-/-}$ mice is not caused by NK cells or type I IFN induction by fibroblasts. The TICAM-1 pathway plays a key role for producing IFN-α/β in Mf/DC, but not in fibroblasts, during PV infection in PVRtg mice.

Discussion

In this study, we demonstrated that PV infection is exacerbated in TICAM-$1^{-/-}$ PVRtg mice. There are a number of RNA-sensing molecules that serve as anti-virus agents and function in a cell type-specific manner. Based on trials using gene-disrupted mice and human viruses, RIG-I has been reported to be essential for sensing infection by rhabdoviruses, influenza viruses, paramyxoviruses, and flaviviruses, whereas MDA5 is important for sensing picornavirus infection (13, 33). In previous studies on picornaviruses, however, only EMCV and several species of picornaviruses have been employed for the KO mice analyses (13). The essential role of type I IFN in PV tropism has been well characterized in PVRtg mice (34). To our knowledge, this study is the first to investigate the sensor that detects PV infection in PVRtg PV-sensitive mice. Because RIG-I and MDA5 use the adaptor IPS-1, we constructed an IPS-$1^{-/-}$ mouse strain for this

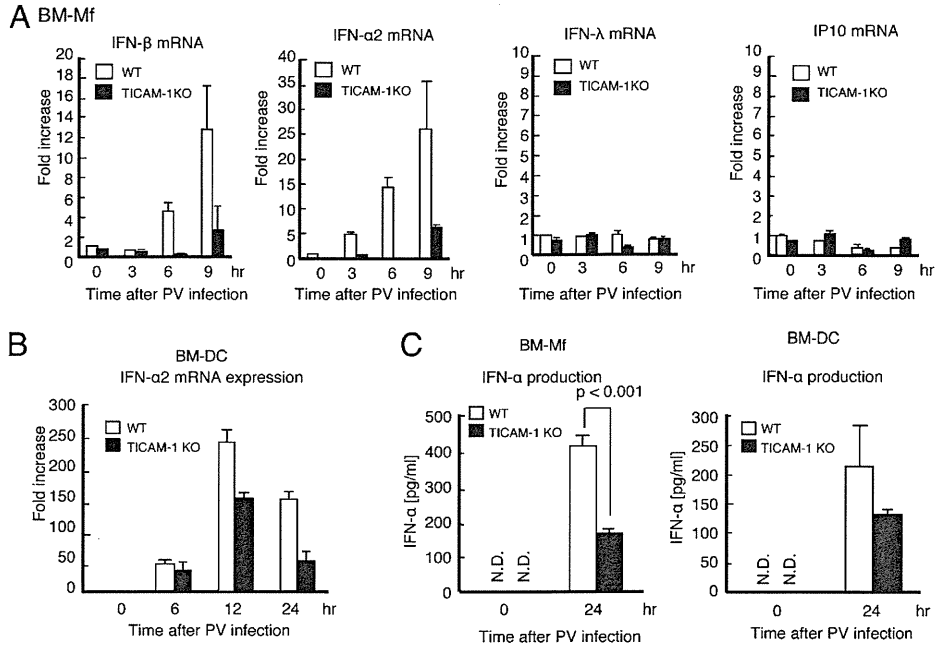

FIGURE 6. Production of type I IFN from BM-Mf and BM-DC. BM-Mf (*A*) and BM-DC (*B*) were prepared from BM cells with M-CSF and GM-CSF, respectively (32). The cells were infected with PV (MOI of 1), and the expression levels of IFN-β, IFN-α2, IFN-λ, and IP-10 were determined by RT-qPCR. *C*, IFN-α produced by PV-infected BM-Mf and BM-DC was measured by ELISA. BM-Mf and BM-DC were prepared from BM cells of WT and TICAM-1$^{-/-}$ mice as in *A* and *B*. Data are shown as means ± SD and are representative of three independent experiments.

study. Unexpectedly, however, IPS-1 was dispensable for protection against PV infection in vivo. This study, taken together with other reports (33, 35, 36), suggests that each virus species has its own strategy to evade host immune attack. This is true even in picornavirus subspecies. Although the IPS-1 pathway involving RIG-I and MDA5 is important for sensing and preventing cytoplasmic virus replication, other steps also participate in critical regulation of virus replication. PV infection is the case where MDA5 is not absolutely critical, but TICAM-1 is essential, for virus protection.

The TICAM-1 pathway participates in driving NK/CTL activation in DC/Mf (21, 37). This pathway is involved in type I IFN induction, as in the IPS-1 pathway, but cells expressing TLR3 are limited. The TLR3 distribution profile by flow cytometry confirms its expression in myeloid cells in mice (30). The TICAM-1 pathway converges with the IPS-1 pathway via the molecular complex of IRF-3–activating kinases (38), and therefore activation of the TICAM-1 pathway induces type I IFN and other IFN-inducible genes (39). Nevertheless, gene induction profiles differ between the TICAM-1 and IPS-1 pathways (40), which may explain the functional distinction between the sensor that is triggered in the virus-infected cells (MDA5/IPS-1) and the sensor that is required for DC/Mf to mount immune responses. Studying these gene functions will be an important issue for functional discrimination between the intrinsic versus extrinsic sensors.

RIG-1/MDA5 are distributed over almost all organs, including Mf/DC. An interesting point concerns what the function is of the IPS-1 pathway in Mf/DC. Without conditional KO mice, we have an experimental limit to discriminate between their intrinsic function that is triggered in PV-infected cells and the extrinsic function leading Mf/DC to driving the innate immune response. Because the TLR3/TICAM-1 pathway is conserved in Mf/DC, the CNS, fibroblasts, and epithelical cells, it is reasonable that their functions are rather specified in Mf/DC and the neuronal system in PV infection.

However, except several examples such as rhabdovirus (41) and hepatitis C virus (HCV) (32), no definitive evidence has been reported supporting the role of TLR3/TICAM-1 in anti-RNA virus function using KO mice, unlike IPS-1 (35, 36). In previous studies, we used RNA viruses and their mouse models of measles virus, respiratory syncitial virus, vesicular stomatitis virus, influenza virus, and rotavirus infection (12), but we were unable to demonstrate solid antiviral function of the TLR3/TICAM-1 pathway in these models (12). Accordingly, which type I IFN, IFN-inducible gene, NK cell, or CTL is an effector for antagonizing viral replication still remains uncharacterized. To our knowledge, the results of our present study first demonstrated that the TLR3/TICAM-1 pathway is indispensable for induction of the type I IFN effector, but not NK cell activation, which is a critical event in the elimination of virus-infected cells and host protection against PV. IL-12 and IFN-γ are not upregulated in splenic DC in a PV-dependent manner. Furthermore, CTL are unlikely to be involved in our present model, since they would not function within the time scale of several days after initial infection (42).

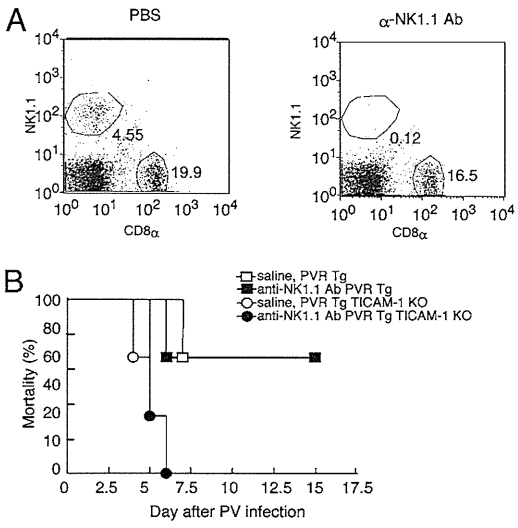

FIGURE 7. Effect of NK cells on mortality of PV-infected TICAM-1$^{-/-}$ PVRtg mice. *A*, To block the NK cell activity in mice, NK1.1 Ab or PBS (control) was i.p. injected into WT mice ($n \geq 6$). After 24 h, spleen cells were isolated from the mice and the fraction of NK1.1$^+$ cells was measured by FACS analysis. *B*, NK1.1 Ab or PBS was i.p. injected into WT and TICAM-1 KO mice. After 24 h, the mice were infected i.p. with PV, and survival was monitored for 15 d.

How PV circumvents host-inducible type I IFN is an intriguing point. Three lines of evidence have supported the presence of unique mechanisms by which PV infection abrogates MDA5-mediated type I IFN production by infected cells and accelerates TLR3-mediated DC maturation through phagocytosis of PV-infected cell debris. First, proteases encoded in the PV genome process the PV polyprotein to produce functional viral proteins (43). PV 2A and 3C proteases also contribute to the degradation of eIF4G (44) and TATA-binding protein (45), respectively, the cleavage of which induces the translational and transcriptional "shutoff" of host protein synthesis (28). Thus, blocking the synthesis of host cell proteins by PV involves stopping IFN production. Second, MDA5 is degraded in PV-infected cells in a proteasome- and caspase-dependent manner, resulting in the lack of type I IFN production (29). Third, PV-mediated apoptosis occurs in a caspase-dependent manner to disable infected cells from inducing an IFN response (46), with the MDA5-dependent innate response to PV infection becoming minimal within 3 h postinfection. Additionally, RIG-I is also cleaved by the viral protease 3C (47), and additional RIG-I functions are subsequently disrupted. Hence, the RIG-I/MDA5 functional time frames should be narrow and ineffective in PV-infected cells.

The hijacked cells release virions and die irrespective of blocking of the IPS-1 pathway. These infected cells are degrading into apoptotic debris containing virus dsRNA when RIG-I/MDA5 is ineffective at inducing IFN (48). Phagocytic internalization of this infected debris containing viral dsRNA into endosomes in Mf/DC is a critical event for TLR3 stimulation (37). If this is the case in PV-infected PVRtg mice, dsRNA-containing debris produced by apoptosis of PV-infected cells may play a major role in the activation of the TICAM-1 pathway in myeloid cells, as is the case for another positive-stranded RNA virus, HCV (32). In HCV studies, dead cells act as carriers of viral dsRNA to the endosomes of DC (32). HCV induces cellular immunity including NK activation driven by the DC TICAM-1 pathway. PV, however, barely induces NK cell activation.

The results of the present study were obtained using the PVRtg mouse model for human PV infection. Possible limitations of this model may include the fact that PV natural infection in humans occurs postinfection of the intestine by a low dose of PV and the PV mouse model is unable to reproduce this infectious route (27). The difference in PV infection between human and the PVRtg mouse might reflect the difference of the IFN-inducing system in humans and mice. However, the response to neurovirulence and death by PV infection occurs similarly in mice and humans. PVRtg mice are susceptible to neuronal infection and the IFNAR$^{-/-}$ phenotype further enhances systemic PV infection (27, 34). The G (Sabin vaccine) and A forms (WT) of PV, which harbor G or A residues in their stem-loop V structures, respectively, show different levels of toxicity or neurovirulence (49). The lower toxicity of the vaccine strain is due to suppression of PTB-mediated protein synthesis in the G form. These results are essentially reproducible in the PVRtg mouse model (50). Our findings further indicate the essential role of the TICAM-1 pathway in the PVRtg model system for the PV-mediated induction of type I IFN in vivo. How this finding is associated with PV-mediated paralytic death and aberrance in the neuronal system is an open question for further understanding the PV neurovirulence and host defense.

In studies on virus infection in neurons, there was no difference between TLR3$^{-/-}$ and WT mice in the brain of reovirus infection (51). TLR3$^{-/-}$ mice have less severe neuroinvasiveness and survive longer than do WT mice in rabies virus infection (41). Further extensive studies have been performed with West Nile virus (WNV). TLR3$^{-/-}$ or TICAM-1$^{-/-}$ mice became more resistant to WNV infection than did WT mice (52). Compared to these earlier results, a recent report showed that lack of TLR3 enhances WNV mortality and increases viral burden in the brain (53). TNF-α and IL-6 are induced for inflammation, and high IL-10 production causes an increase of mortality in WNV-infected mice (54). TICAM-1 signaling is undoubtedly involved in the modulation of these cytokine productions and WNV replication in the nervous system (53, 54). In patients with herpes simplex encephalitis, functional deficiency of TLR3 or TICAM-1 is a critical factor for disease progression (55). The TLR3 responses in the CNS may differ from those in the immune system we examined (54, 56). How PV infection modulates IFN/cytokine-inducing signaling in the nervous system is an interesting issue. The possibility remains that cytokines, such as TNF-α, IL-10, IL-12p40, and IFN-γ, might be associated with the removal of infectious cells as in other virus infections, and the antiviral function of TLR3 ligands in PV-infected mice requires further elucidation.

A picornavirus CBV activates the TLR3/TICAM-1–IFN-γ axis in host-infected cells to induce type II IFN (18). It is possible that CBV promotes TLR3-dependent IFN-γ induction in lymphocytes rather than the type I IFN-inducing pathway. In the model of PV infection, however, the TICAM-1 pathway does not contribute to type II IFN induction. These findings indicate that picornaviruses, that is, EMCV, CBV and PV, have independently evolved to adapt to the host innate immune system and cope with the IFN-inducing system. If this is the case, host responses against picornaviruses may not be unimodally raised by MDA5 but may provide differentially adapted strategies. EMCV tropism reported previously (13) is clearly distinct from those of other picornaviruses. In this article, we present evidence that PV infection is protected by the TICAM-1 pathway that extrinsically induces type I IFN. Virus-produced dsRNA may differentially act on host cells depending on each virus species and accomplish circumvention from host innate sensing systems, maintaining virus tropism.

Acknowledgments

We are grateful to Dr. A. Nomoto (University of Tokyo, Tokyo, Japan) and our laboratory members for invaluable discussions. We also thank Dr. D.M. Segal (National Institutes of Health, Bethesda, MD) for providing the anti-mouse TLR3 mAb and Drs. S. Akira (Osaka University, Osaka, Japan) and T. Taniguchi (University of Tokyo) for providing TLR3$^{-/-}$ and IRF3/7$^{-/-}$ mice, respectively, for this study.

Disclosures

The authors have no financial conflicts of interest.

References

1. Takeuchi, O., and S. Akira. 2009. Innate immunity to virus infection. *Immunol. Rev.* 227: 75–86.
2. Malathi, K., B. Dong, M. Gale, Jr., and R. H. Silverman. 2007. Small self-RNA generated by RNase L amplifies antiviral innate immunity. *Nature* 448: 816–819.
3. Oshiumi, H., M. Matsumoto, K. Funami, T. Akazawa, and T. Seya. 2003. TICAM-1, an adaptor molecule that participates in Toll-like receptor 3-mediated interferon-β induction. *Nat. Immunol.* 4: 161–167.
4. Yamamoto, M., S. Sato, H. Hemmi, K. Hoshino, T. Kaisho, H. Sanjo, O. Takeuchi, M. Sugiyama, M. Okabe, K. Takeda, and S. Akira. 2003. Role of adaptor TRIF in the MyD88-independent Toll-like receptor signaling pathway. *Science* 301: 640–643.
5. Hoebe, K., X. Du, P. Georgel, E. Janssen, K. Tabeta, S. O. Kim, J. Goode, P. Lin, N. Mann, S. Mudd, et al. 2003. Identification of Lps2 as a key transducer of MyD88-independent TIR signalling. *Nature* 424: 743–748.
6. Akira, S. 2003. Toll-like receptor signaling. *J. Biol. Chem.* 278: 38105–38108.
7. Matsumoto, M., and T. Seya. 2008. TLR3: interferon induction by double-stranded RNA including poly(I:C). *Adv. Drug Deliv. Rev.* 60: 805–812.
8. Funami, K., M. Sasai, Y. Ohba, H. Oshiumi, T. Seya, and M. Matsumoto. 2007. Spatiotemporal mobilization of Toll/IL-1 receptor domain-containing adaptor molecule-1 in response to dsRNA. *J. Immunol.* 179: 6867–6872.
9. Funami, K., M. Sasai, H. Oshiumi, T. Seya, and M. Matsumoto. 2008. Homo-oligomerization is essential for Toll/interleukin-1 receptor domain-containing

adaptor molecule-1-mediated NF-κB and interferon regulatory factor-3 activation. *J. Biol. Chem.* 283: 18283–18291.
10. Yoneyama, M., M. Kikuchi, T. Natsukawa, N. Shinobu, T. Imaizumi, M. Miyagishi, K. Taira, S. Akira, and T. Fujita. 2004. The RNA helicase RIG-I has an essential function in double-stranded RNA-induced innate antiviral responses. *Nat. Immunol.* 5: 730–737.
11. Yoneyama, M., M. Kikuchi, K. Matsumoto, T. Imaizumi, M. Miyagishi, K. Taira, E. Foy, Y. M. Loo, M. Gale, Jr., S. Akira, et al. 2005. Shared and unique functions of the DExD/H-box helicases RIG-I, MDA5, and LGP2 in antiviral innate immunity. *J. Immunol.* 175: 2851–2858.
12. Matsumoto, M., H. Oshiumi, and T. Seya. 2011. Antiviral responses induced by the TLR3 pathway. *Rev. Med. Virol.* 21: 67–77.
13. Kato, H., O. Takeuchi, S. Sato, M. Yoneyama, M. Yamamoto, K. Matsui, S. Uematsu, A. Jung, T. Kawai, K. J. Ishii, et al. 2006. Differential roles of MDA5 and RIG-I helicases in the recognition of RNA viruses. *Nature* 441: 101–105.
14. Tabeta, K., P. Georgel, E. Janssen, X. Du, K. Hoebe, K. Crozat, S. Mudd, L. Shamel, S. Sovath, J. Goode, et al. 2004. Toll-like receptors 9 and 3 as essential components of innate immune defense against mouse cytomegalovirus infection. *Proc. Natl. Acad. Sci. USA* 101: 3516–3521.
15. Baltimore, D., Y. Becker, and J. E. Darnell. 1964. Virus-specific double-stranded RNA in poliovirus-infected cells. *Science* 143: 1034–1036.
16. Nomoto, A., B. Detjen, R. Pozzatti, and E. Wimmer. 1977. The location of the polio genome protein in viral RNAs and its implication for RNA synthesis. *Nature* 268: 208–213.
17. Gitlin, L., W. Barchet, S. Gilfillan, M. Cella, B. Beutler, R. A. Flavell, M. S. Diamond, and M. Colonna. 2006. Essential role of mda-5 in type I IFN responses to polyriboinosinic:polyribocytidylic acid and encephalomyocarditis picornavirus. *Proc. Natl. Acad. Sci. USA* 103: 8459–8464.
18. Negishi, H., T. Osawa, K. Ogami, X. Ouyang, S. Sakaguchi, R. Koshiba, H. Yanai, Y. Seko, H. Shitara, K. Bishop, et al. 2008. A critical link between Toll-like receptor 3 and type II interferon signaling pathways in antiviral innate immunity. *Proc. Natl. Acad. Sci. USA* 105: 20446–20451.
19. Ren, R. B., F. Costantini, E. J. Gorgacz, J. J. Lee, and V. R. Racaniello. 1990. Transgenic mice expressing a human poliovirus receptor: a new model for poliomyelitis. *Cell* 63: 353–362.
20. Koike, S., C. Taya, T. Kurata, S. Abe, I. Ise, H. Yonekawa, and A. Nomoto. 1991. Transgenic mice susceptible to poliovirus. *Proc. Natl. Acad. Sci. USA* 88: 951–955.
21. Akazawa, T., T. Ebihara, M. Okuno, Y. Okuda, M. Shingai, K. Tsujimura, T. Takahashi, M. Ikawa, M. Okabe, N. Inoue, et al. 2007. Antitumor NK activation induced by the Toll-like receptor 3-TICAM-1 (TRIF) pathway in myeloid dendritic cells. *Proc. Natl. Acad. Sci. USA* 104: 252–257.
22. Honda, K., H. Yanai, H. Negishi, M. Asagiri, M. Sato, T. Mizutani, N. Shimada, Y. Ohba, A. Takaoka, N. Yoshida, and T. Taniguchi. 2005. IRF-7 is the master regulator of type-I interferon-dependent immune responses. *Nature* 434: 772–777.
23. Kato, H., O. Takeuchi, E. Mikamo-Satoh, R. Hirai, T. Kawai, K. Matsushita, A. Hiiragi, T. S. Dermody, T. Fujita, and S. Akira. 2008. Length-dependent recognition of double-stranded ribonucleic acids by retinoic acid-inducible gene-I and melanoma differentiation-associated gene 5. *J. Exp. Med.* 205: 1601–1610.
24. Hornung, V., J. Ellegast, S. Kim, K. Brzózka, A. Jung, H. Kato, H. Poeck, S. Akira, K. K. Conzelmann, M. Schlee, et al. 2006. 5′-Triphosphate RNA is the ligand for RIG-I. *Science* 314: 994–997.
25. Pichlmair, A., O. Schulz, C. P. Tan, T. I. Näslund, P. Liljeström, F. Weber, and C. Reis e Sousa. 2006. RIG-I-mediated antiviral responses to single-stranded RNA bearing 5′-phosphates. *Science* 314: 997–1001.
26. Nakajima, A., K. Nishimura, Y. Nakaima, T. Oh, S. Noguchi, T. Taniguchi, and T. Tamura. 2009. Cell type-dependent proapoptotic role of Bcl2L12 revealed by a mutation concomitant with the disruption of the juxtaposed *Irf3* gene. *Proc. Natl. Acad. Sci. USA* 106: 12448–12452.
27. Ohka, S., H. Igarashi, N. Nagata, M. Sakai, S. Koike, T. Nochi, H. Kiyono, and A. Nomoto. 2007. Establishment of a poliovirus oral infection system in human poliovirus receptor-expressing transgenic mice that are deficient in α/β interferon receptor. *J. Virol.* 81: 7902–7912.
28. Racaniello, V. R. 2007. Picornaviridae: the viruses and their replication. In *Fields Virology*, 5th Ed. D. M. Knipe and P. M. Howley, eds. Lippincott Williams & Wilkins, Philadelphia, p. 795–838.
29. Barral, P. M., J. M. Morrison, J. Drahos, P. Gupta, D. Sarkar, P. B. Fisher, and V. R. Racaniello. 2007. MDA-5 is cleaved in poliovirus-infected cells. *J. Virol.* 81: 3677–3684.
30. Jelinek, I., J. N. Leonard, G. E. Price, K. N. Brown, A. Meyer-Manlapat, P. K. Goldsmith, Y. Wang, D. Venzon, S. L. Epstein, and D. M. Segal. 2011. TLR3-specific double-stranded RNA oligonucleotide adjuvants induce dendritic cell cross-presentation, CTL responses, and antiviral protection. *J. Immunol.* 186: 2422–2429.
31. Matsumoto, M., K. Funami, M. Tanabe, H. Oshiumi, M. Shingai, Y. Seto, A. Yamamoto, and T. Seya. 2003. Subcellular localization of Toll-like receptor 3 in human dendritic cells. *J. Immunol.* 171: 3154–3162.
32. Ebihara, T., M. Shingai, M. Matsumoto, T. Wakita, and T. Seya. 2008. Hepatitis C virus-infected hepatocytes extrinsically modulate dendritic cell maturation to activate T cells and natural killer cells. *Hepatology* 48: 48–58.
33. Loo, Y. M., J. Fornek, N. Crochet, G. Bajwa, O. Perwitasari, L. Martinez-Sobrido, S. Akira, M. A. Gill, A. García-Sastre, M. G. Katze, and M. Gale, Jr. 2008. Distinct RIG-I and MDA5 signaling by RNA viruses in innate immunity. *J. Virol.* 82: 335–345.
34. Ida-Hosonuma, M., T. Iwasaki, T. Yoshikawa, N. Nagata, Y. Sato, T. Sata, M. Yoneyama, T. Fujita, C. Taya, H. Yonekawa, and S. Koike. 2005. The α/β interferon response controls tissue tropism and pathogenicity of poliovirus. *J. Virol.* 79: 4460–4469.
35. Kumar, H., T. Kawai, H. Kato, S. Sato, K. Takahashi, C. Coban, M. Yamamoto, S. Uematsu, K. J. Ishii, O. Takeuchi, and S. Akira. 2006. Essential role of IPS-1 in innate immune responses against RNA viruses. *J. Exp. Med.* 203: 1795–1803.
36. Sun, Q., L. Sun, H. H. Liu, X. Chen, R. B. Seth, J. Forman, and Z. J. Chen. 2006. The specific and essential role of MAVS in antiviral innate immune responses. *Immunity* 24: 633–642.
37. Schulz, O., S. S. Diebold, M. Chen, T. I. Näslund, M. A. Nolte, L. Alexopoulou, Y. T. Azuma, R. A. Flavell, P. Liljeström, and C. Reis e Sousa. 2005. Toll-like receptor 3 promotes cross-priming to virus-infected cells. *Nature* 433: 887–892.
38. Sasai, M., M. Shingai, K. Funami, M. Yoneyama, T. Fujita, M. Matsumoto, and T. Seya. 2006. NAK-associated protein 1 participates in both the TLR3 and the cytoplasmic pathways in type I IFN induction. *J. Immunol.* 177: 8676–8683.
39. Oshiumi, H., M. Sasai, K. Shida, T. Fujita, M. Matsumoto, and T. Seya. 2003. TIR-containing adapter molecule (TICAM)-2, a bridging adapter recruiting to Toll-like receptor 4 TICAM-1 that induces interferon-beta. *J. Biol. Chem.* 278: 49751–49762.
40. Ueta, M., T. Kawai, N. Yokoi, S. Akira, and S. Kinoshita. 2011. Contribution of IPS-1 to polyI:C-induced cytokine production in conjunctival epithelial cells. *Biochem. Biophys. Res. Commun.* 404: 419–423.
41. Ménager, P., P. Roux, F. Mégret, J. P. Bourgeois, A. M. Le Sourd, A. Danckaert, M. Lafage, C. Préhaud, and M. Lafon. 2009. Toll-like receptor 3 (TLR3) plays a major role in the formation of rabies virus Negri bodies. *PLoS Pathog.* 5: e1000315.
42. Sigal, L. J., S. Crotty, R. Andino, and K. L. Rock. 1999. Cytotoxic T-cell immunity to virus-infected non-haematopoietic cells requires presentation of exogenous antigen. *Nature* 398: 77–80.
43. Nicklin, M. J., H. G. Kräusslich, H. Toyoda, J. J. Dunn, and E. Wimmer. 1987. Poliovirus polypeptide precursors: expression in vitro and processing by exogenous 3C and 2A proteinases. *Proc. Natl. Acad. Sci. USA* 84: 4002–4006.
44. Kräusslich, H. G., M. J. Nicklin, H. Toyoda, D. Etchison, and E. Wimmer. 1987. Poliovirus proteinase 2A induces cleavage of eucaryotic initiation factor 4F polypeptide p220. *J. Virol.* 61: 2711–2718.
45. Clark, M. E., P. M. Lieberman, A. J. Berk, and A. Dasgupta. 1993. Direct cleavage of human TATA-binding protein by poliovirus protease 3C in vivo and in vitro. *Mol. Cell. Biol.* 13: 1232–1237.
46. Belov, G. A., L. I. Romanova, E. A. Tolskaya, M. S. Kolesnikova, Y. A. Lazebnik, and V. I. Agol. 2003. The major apoptotic pathway activated and suppressed by poliovirus. *J. Virol.* 77: 45–56.
47. Barral, P. M., D. Sarkar, P. B. Fisher, and V. R. Racaniello. 2009. RIG-I is cleaved during picornavirus infection. *Virology* 391: 171–176.
48. Barco, A., E. Feduchi, and L. Carrasco. 2000. Poliovirus protease $3C^{pro}$ kills cells by apoptosis. *Virology* 266: 352–360.
49. Kawamura, N., M. Kohara, S. Abe, T. Komatsu, K. Tago, M. Arita, and A. Nomoto. 1989. Determinants in the 5′ noncoding region of poliovirus Sabin 1 RNA that influence the attenuation phenotype. *J. Virol.* 63: 1302–1309.
50. Koike, S., H. Horie, Y. Sato, I. Ise, C. Taya, T. Nomura, I. Yoshioka, H. Yonekawa, and A. Nomoto. 1993. Poliovirus-sensitive transgenic mice as a new animal model. *Dev. Biol. Stand.* 78: 101–107.
51. Edelmann, K. H., S. Richardson-Burns, L. Alexopoulou, K. L. Tyler, R. A. Flavell, and M. B. A. Oldstone. 2004. Does Toll-like receptor 3 play a biological role in virus infections? *Virology* 322: 231–238.
52. Wang, T., T. Town, L. Alexopoulou, J. F. Anderson, E. Fikrig, and R. A. Flavell. 2004. Toll-like receptor 3 mediates West Nile virus entry into the brain causing lethal encephalitis. *Nat. Med.* 10: 1366–1373.
53. Daffis, S., M. A. Samuel, M. S. Suthar, M. Gale, Jr., and M. S. Diamond. 2008. Toll-like receptor 3 has a protective role against West Nile virus infection. *J. Virol.* 82: 10349–10358.
54. Bai, F., T. Town, F. Qian, P. Wang, M. Kamanaka, T. M. Connolly, D. Gate, R. R. Montgomery, R. A. Flavell, and E. Fikrig. 2009. IL-10 signaling blockade controls murine West Nile virus infection. *PLoS Pathog.* 5: e1000610.
55. Zhang, S. Y., E. Jouanguy, S. Ugolini, A. Smahi, G. Elain, P. Romero, D. Segal, V. Sancho-Shimizu, L. Lorenzo, A. Puel, et al. 2007. TLR3 deficiency in patients with herpes simplex encephalitis. *Science* 317: 1522–1527.
56. Préhaud, C., F. Mégret, M. Lafage, and M. Lafon. 2005. Virus infection switches TLR-3-positive human neurons to become strong producers of beta interferon. *J. Virol.* 79: 12893–12904.

MOLECULAR AND CELLULAR BIOLOGY, Sept. 2011, p. 3802–3819 Vol. 31, No. 18
0270-7306/11/$12.00 doi:10.1128/MCB.01368-10

DDX60, a DEXD/H Box Helicase, Is a Novel Antiviral Factor Promoting RIG-I-Like Receptor-Mediated Signaling▽†

Moeko Miyashita,[1,2] Hiroyuki Oshiumi,[1]* Misako Matsumoto,[1] and Tsukasa Seya[1]

Department of Microbiology and Immunology, Graduate School of Medicine,[1] and Graduate School of Life Science,[2] Hokkaido University, Kita-15, Nishi-7, Kita-ku, Sapporo 060-8638, Japan

Received 30 November 2010/Returned for modification 27 December 2010/Accepted 12 July 2011

The cytoplasmic viral RNA sensors RIG-I and MDA5 are important for the production of type I interferon and other inflammatory cytokines. DDX60 is an uncharacterized DEXD/H box RNA helicase similar to *Saccharomyces cerevisiae* Ski2, a cofactor of RNA exosome, which is a protein complex required for the integrity of cytoplasmic RNA. Expression of DDX60 increases after viral infection, and the protein localizes at the cytoplasmic region. After viral infection, the DDX60 protein binds to endogenous RIG-I protein. The protein also binds to MDA5 and LGP2 but not to the downstream factors IPS-1 and IκB kinase ε (IKK-ε). Knockdown analysis shows that DDX60 is required for RIG-I- or MDA5-dependent type I interferon and interferon-inducible gene expression in response to viral infection. However, DDX60 is dispensable for TLR3-mediated signaling. Purified DDX60 helicase domains possess the activity to bind to viral RNA and DNA. Expression of DDX60 promotes the binding of RIG-I to double-stranded RNA. Taken together, our analyses indicate that DDX60 is a novel antiviral helicase promoting RIG-I-like receptor-mediated signaling.

RIG-I and MDA5 are cytoplasmic viral RNA sensors belonging to the group of RIG-I-like receptors (RLRs), which includes LGP2 (57–59). RIG-I recognizes RNAs from vesicular stomatitis virus (VSV), hepatitis C virus (HCV), Sendai virus (SeV), and influenza A virus (21, 36, 37), while MDA5 recognizes RNA from picornaviruses such as encephalomyocarditis virus and poliovirus (PV) (3, 19, 21). RLRs are also involved in the recognition of cytoplasmic B-DNA. RNA polymerase III transcribes cytoplasmic AT-rich double-stranded DNA (dsDNA), and the transcribed RNA is recognized by RIG-I (1, 6). In contrast, Choi et al. have reported that RIG-I associates with dsDNA (7).

When RIG-I or MDA5 is activated by viral infection, the N-terminal caspase recruitment domains (CARDs) associate with the adaptor protein IPS-1 (also called MAVS/Cardif/VISA) on the outer mitochondrial membrane (22, 26, 42, 55). After this association occurs, IPS-1 activates TBK1 and IκB kinase ε (IKK-ε) and signals interferon (IFN) regulatory factor 3 (IRF-3)- and NF-κB-responsive genes, such as those for type I IFNs or other inflammatory cytokines (22, 23, 26, 42, 44, 55).

Both the helicase and C-terminal domain (CTD) of RIG-I bind to RNA, but it is the CTD that is responsible for the recognition of the 5′ triphosphate double-stranded structure typical of viral RNA (16, 39, 40). Recently, Rehwinkel et al. showed that the physiological ligand of RIG-I during influenza A virus or SeV infection is the full-length viral genomic single-stranded RNA (ssRNA), which possesses base-paired regions or defective interfering (DI) genomes (35). In contrast to RIG-I, MDA5 recognizes long viral double-stranded RNA (dsRNA) (21). The RNA binding activity of the MDA5 CTD is relatively weak compared with that of the RIG-I CTD, because the basic surface of the MDA5 CTD has a more extensive flat region than the RIG-I CTD (8, 45, 46). Although the RNA binding activity of the MDA5 CTD is weak, this protein plays a pivotal role in the recognition of picornavirus RNA (20, 21).

For the efficient recognition of viral RNA, RIG-I and MDA5 require protein modification and association with upstream factors. LGP2 is one of the upstream factors. LGP2 lacks an N-terminal CARD; thus, LGP2 itself cannot transmit the signal in the absence of RIG-I or MDA5 (36, 38, 49). The CTD of LGP2, which binds to the terminal region of viral double-stranded RNA, is more similar to the CTD of RIG-I than to that of MDA5 (24, 33, 45). LGP2 knockout studies have revealed that LGP2 is essential for type I IFN production by MDA5 but plays only a minor role in type I IFN production by RIG-I (38, 49). RIG-I requires modification of K63-linked polyubiquitination by TRIM25 and Riplet/REUL ubiquitin ligases for its full activation (11, 13, 30, 31). High-mobility-group box (HMGB) proteins also act as upstream factors of RLRs. Recently, Yanai and colleagues reported that HMGB1, HMGB2, and HMGB3 serve as sentinels for the nucleic acids required for both RIG-I and MDA5 recognition of viral RNA (56). Hayakawa and colleagues reported that ZAPS associates with RIG-I to promote oligomerization and ATPase activity of RIG-I (15). Another factor interacting with RLRs is DDX3, a DEXD/H box RNA helicase, which is similar to LGP2 in that it does not contain a CARD but promotes signaling by forming a complex with either RIG-I or MDA5 (32). DDX3 also plays important roles in TBK-1- and IKK-ε-mediated IRF activation, and Schröder et al. and Soulat et al. were the first to describe results showing that DDX3 is a non-RLR helicase involved in innate immune responses (41, 43).

DDX60, a DEXD/H box helicase, was annotated in a genome project, and the protein function is unknown. The protein is weakly similar to SKIV2L and SKIV2L2 and is the

* Corresponding author. Mailing address: Department of Microbiology and Immunology, Graduate School of Medicine, Hokkaido University, Kita-15, Nishi-7, Kita-ku, Sapporo 060-8638, Japan. Phone: 81-11-706-5056. Fax: 81-11-706-7866. E-mail: oshiumi@med.hokudai.ac.jp.

† Supplemental material for this article may be found at http://mcb.asm.org/.

▽ Published ahead of print on 2 May 2011.

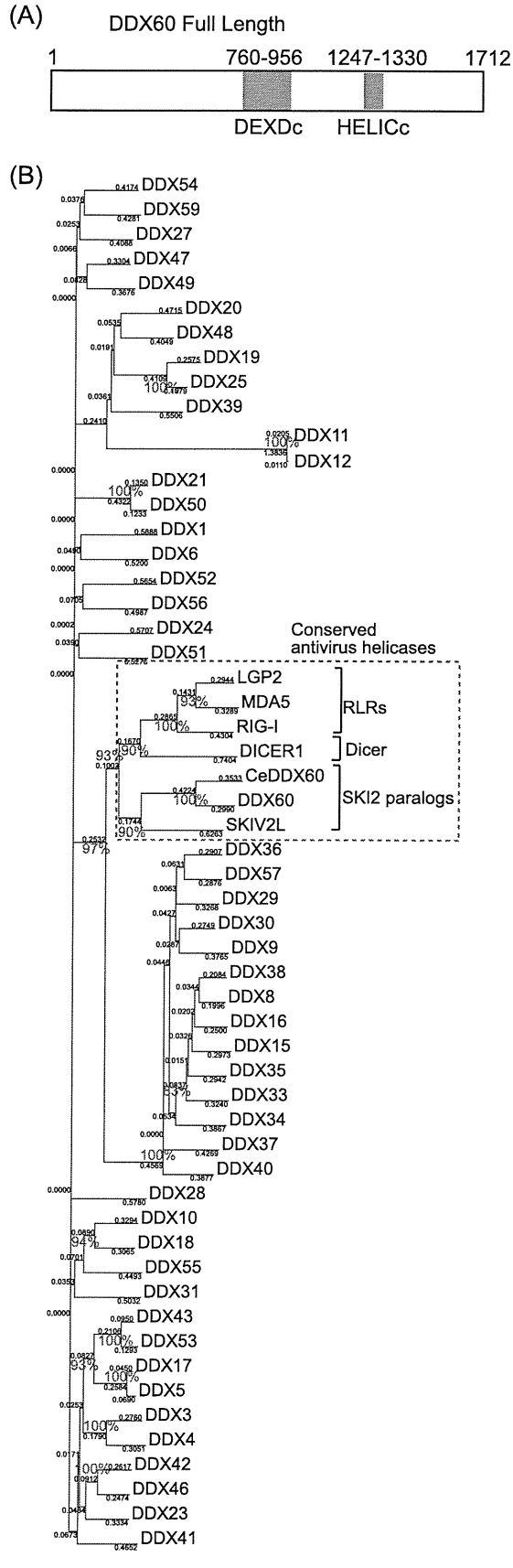

human homolog of *Saccharomyces cerevisiae* (budding yeast) Ski2, a cofactor of the RNA exosome (9, 18). The RNA exosome is a macromolecular protein complex that includes ribonucleases and helicases and controls the quality of host RNA molecules in both the nucleus and cytoplasm (17). It is composed of nine core components and several cofactor proteins (18). In budding yeast, the RNA exosome and Ski2 together exhibit antiviral activity (53, 54); similarly, the mammalian RNA exosome, together with its cofactors, shows antiviral activity against Moloney leukemia virus and Sindbis virus (5, 14). Our microarray analysis has shown that DDX60 is upregulated in human dendritic cells during infection with measles virus (MV) (our unpublished results). Thus, we expected DDX60 to be a novel antiviral protein and found that DDX60 is involved in RIG-I-like receptor-dependent antiviral pathways.

Here, we show that DDX60 is induced during viral infection and suppresses viral replication. DDX60 was found to form a complex with RLRs, promoting signaling; the results of knockdown experiments indicated that DDX60 is involved in RLR-dependent pathways. Moreover, the DDX60 helicase domain was observed to bind to viral RNA and DNA. Furthermore, DDX60 is required for type I IFN expression after DNA virus infection. These data indicate that DDX60 is a novel antiviral helicase involved in RLR-dependent pathways.

MATERIALS AND METHODS

Cell cultures. HEK293 and Vero cells were cultured in Dulbecco's modified Eagle's medium with 10% heat-inactivated fetal calf serum (Invitrogen), and HeLa cells were cultured in minimum Eagle's medium with 2 mM L-glutamine and 10% heat-inactivated fetal calf serum (JRH Biosciences). HEK293FT cells were maintained in Dulbecco's modified Eagle's high-glucose medium containing 10% heat-inactivated fetal calf serum (Invitrogen). RAW 264.7 cells were cultured in RPMI 1640 medium with 10% heat-inactivated fetal calf serum (Invitrogen). Mouse bone marrow-derived dendritic cells (BM-DCs) were induced as described in reference 2. PV receptor (PVR)-transgenic mice were provided by S. Koike (Tokyo Metropolitan Institute for Neuroscience).

Plasmids. Full-length human DDX60 cDNA was obtained from HeLa cell total RNA by reverse transcription-PCR (RT-PCR). The obtained cDNA fragments were sequenced, and we confirmed by PCR that the obtained cDNA clones do not contain nucleotide mutations. The DDX60 cDNA clone was cloned into XhoI and NotI restriction sites of pEF-BOS, and a hemagglutinin (HA) tag sequence was inserted just before the stop codon. EXOSC1, EXOSC4, or EXOSC5 was amplified by RT-PCR from HeLa cell total RNA. The obtained cDNA fragment was cloned into XhoI and NotI restriction sites of pEF-BOS vector, and the FLAG tag was fused at the C-terminal end. The DDX6 cDNA carrying a full-length open reading frame (ORF) was amplified by RT-PCR using primers DDX6-F (GGC CGC TCG AGC CAC CAT GAG CAC GGC CAG AAC AGA G) and DDX6-R (GGC GGG GTA CCC CAG GTT TCT CAT CTT CTA CAG). The fragment was cloned into XhoI and NotI sites of pEF-BOS vector. For *in vitro* viral RNA synthesis, we amplified VSV-G region cDNA by PCR using primers VSV-G-F and VSV-G-R. The obtained cDNA fragment was cloned into pGEM-T Easy vector. The primer sequences are as follows: for VSV-G-F, ACAGGAGAATGGGTTGATTC; and for VSV-G-R, ATGCAAA GATGGATACCAAC. Vectors expressing full RIG-I or RIG-I fragments were described before (30). The plasmids expressing TLR3 or TICAM-1 are described in reference 29. The p125luc reporter plasmid was a gift from T. Taniguchi (University of Tokyo, Tokyo, Japan). Mutant DDX60 expression constructs were

FIG. 1. The phylogenetic tree of DEXD/H box RNA helicase. (A) Schematic diagram of DDX60. DDX60 encodes a peptide of 1,712 amino acids (aa) that contains a DEXD/H box (DEXDc; aa 760 to 956) and HELICc (aa 1247 to 1330). (B) The phylogenetic tree of DEXD/H box RNA heliases. Ce, *C. elegans*. The bootstrap probabilities and genetic distances are shown in red and black, respectively.

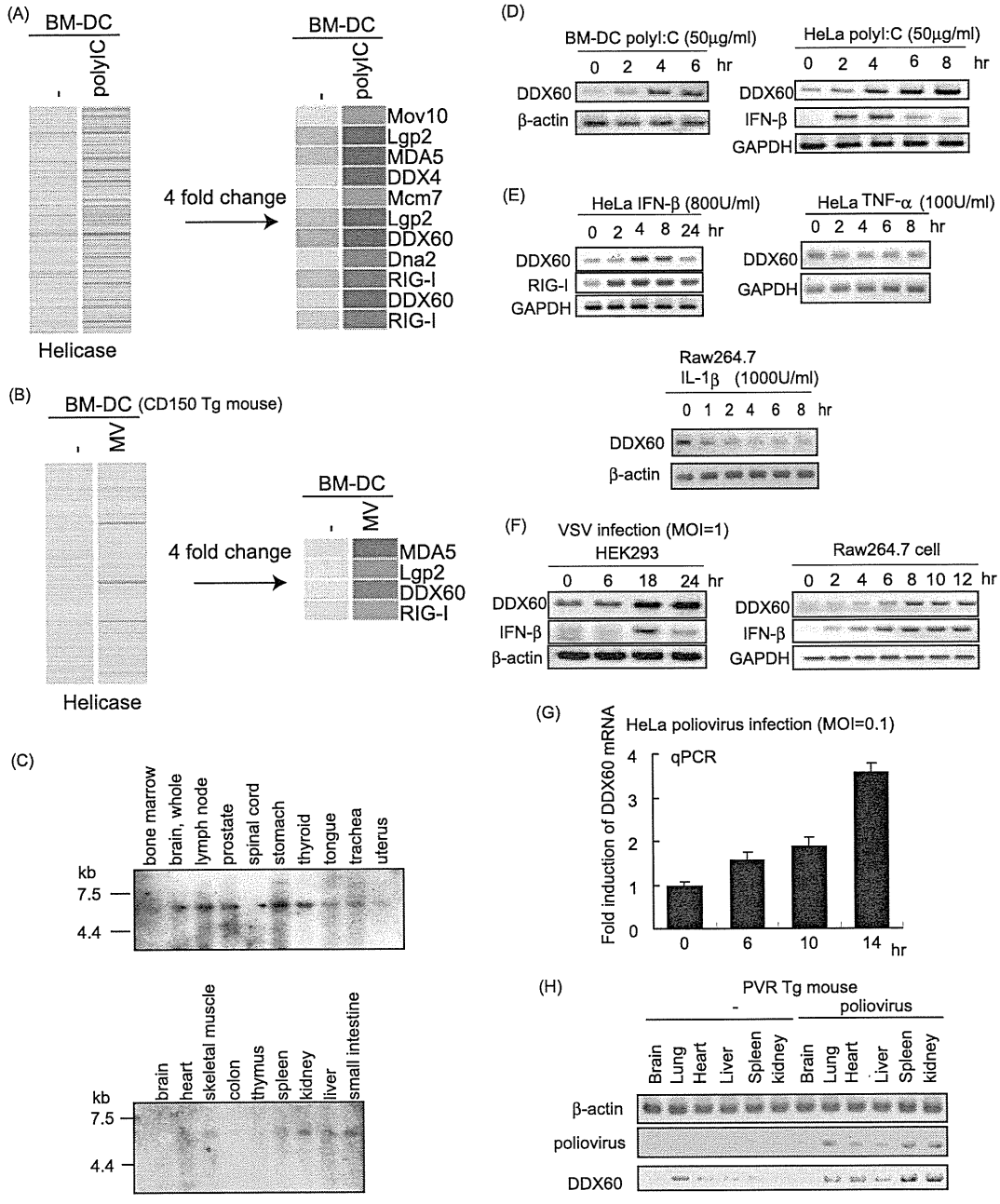

FIG. 2. Expression of DDX60 mRNA. (A and B) Mouse BM-DCs were stimulated with poly(I · C) (A) or infected with MV in the presence of anti-IFN-AR antibody (B). Total RNA was extracted from the cells, and microarray analysis was performed. The heat maps in the left column show the expression profiles of the genes encoding the helicase domain. The heat maps in the right column show the genes encoding the helicase domain whose expression levels changed more than 4-fold. (C) Northern blot of human DDX60 mRNAs in specified tissues. Northern blots of human tissues were probed with DDX60 cDNA. (D and E) Mouse BM-DCs, HeLa cells, or RAW 264.7 cells were stimulated with 50 μg of poly(I · C)/ml (D), 800 U of IFN-β/ml (E), 100 U of TNF-α/ml (E), or 1,000 U of IL-1β/ml (E). Expression of DDX60, RIG-I, GAPDH (glyceraldehyde-3-phosphate dehydrogenase), and β-actin mRNA was examined by RT-PCR. (F and G) HEK293 cells, RAW 264.7 cells, or HeLa cells were infected with VSV at an MOI of 1 (F) or PV at an MOI of 0.1 (G). Expression of DDX60, IFN-β, β-actin, and/or GAPDH was examined by RT-PCR (F) or RT-qPCR (G). (H) PV was injected intraperitoneally (i.p.) into PVR-transgenic mice susceptible to PV. Tissue RNA extraction was performed before or 3 days after infection, and RT-PCR was carried out on these samples.

amplified using primers for DDX60 (amino acids [aa] 1 to 169), (aa 169 to 334), (aa 334 to 490), (aa 478 to 656), (aa 657 to 857), (aa 857 to 1054), (aa 1049 to 1256), (aa 1256 to 1409), (aa 1407 to 1543), and (aa 1543 to 1712). The primer sequences are shown in Table S1 in the supplemental material.

Phylogenetic analysis. The amino acid sequences of the DEXD/H box domain were aligned using ClustalW software on the NIG server. The phylogenetic tree was drawn using the neighbor-joining method and GENETYX-MAC software (version 13.0.3).

Northern blotting. A human DDX60 644-bp cDNA fragment (from the region at bp 3978 to 4621) was used for the probe for Northern blotting. The Northern blot membranes (human 12-lane multiple-tissue Northern [MTN] blot and MTN blot III) were purchased from Clontech. The probe was labeled using

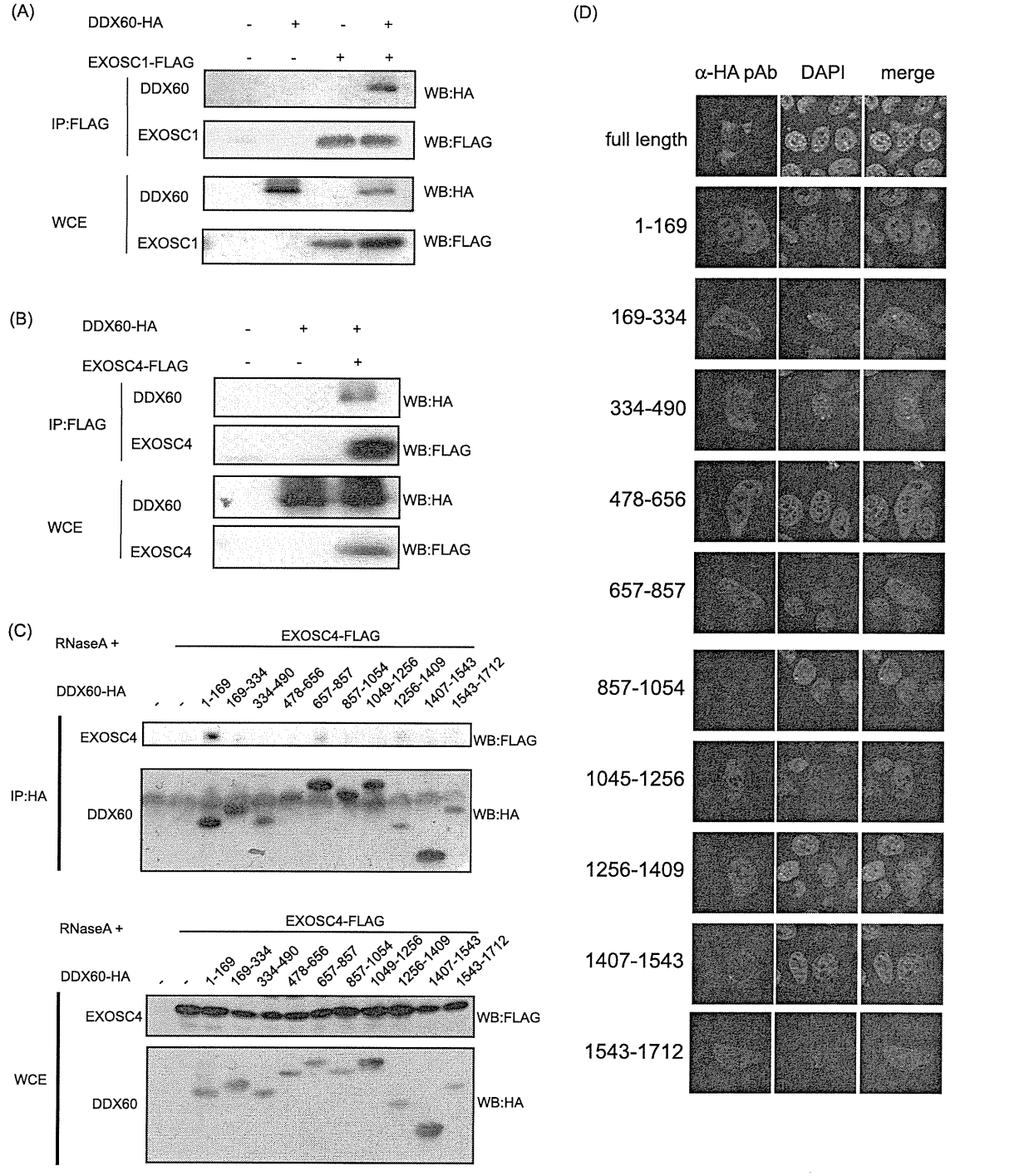

FIG. 3. Interactions between DDX60 and RNA exosome components. (A and B) HA-tagged DDX60 and FLAG-tagged EXOSC1 (A) and EXOSC4 (B) expression vector was transfected into HEK293FT cells. After 24 h, cell lysates were prepared and immunoprecipitation (IP) was performed with anti-FLAG antibody. The samples were analyzed by SDS-PAGE and detected by Western blotting (WB) using anti-HA or anti-FLAG antibodies. WCE, whole-cell extract (WCE). (C) HA-tagged DDX60 partial fragments and/or FLAG-tagged EXOSC4 expression vectors were transfected into HEK293FT cells, and immunoprecipitation was carried out as described for panel A in the presence of RNase A. (D) HA-tagged DDX60 fragment-expressing vectors were transfected into HeLa cells. The cells were stained with anti-HA antibody and DAPI and then observed by confocal microscopy.

[α-^{32}P]dCTP and a Rediprime II random prime labeling system (GE Healthcare). The labeled probe was hybridized to the membrane by the use of ExpressHyb hybridization solution (Clontech) at 68°C for 1 h. The membrane was washed with washing solution I (2× SSC [1× SSC is 0.15 M NaCl plus 0.015 M sodium citrate], 0.05% sodium dodecyl sulfate [SDS]) for 40 min and then washed with washing solution II (0.1× SSC, 0.1% SDS) for 40 min. DDX60 mRNA bands were detected with X-ray film.

RT-PCR and real-time PCR. Total RNA was extracted with TRIzol reagent (Invitrogen), and then the samples were treated with DNase I to remove the DNA contamination. The reverse transcription reaction was carried out using a

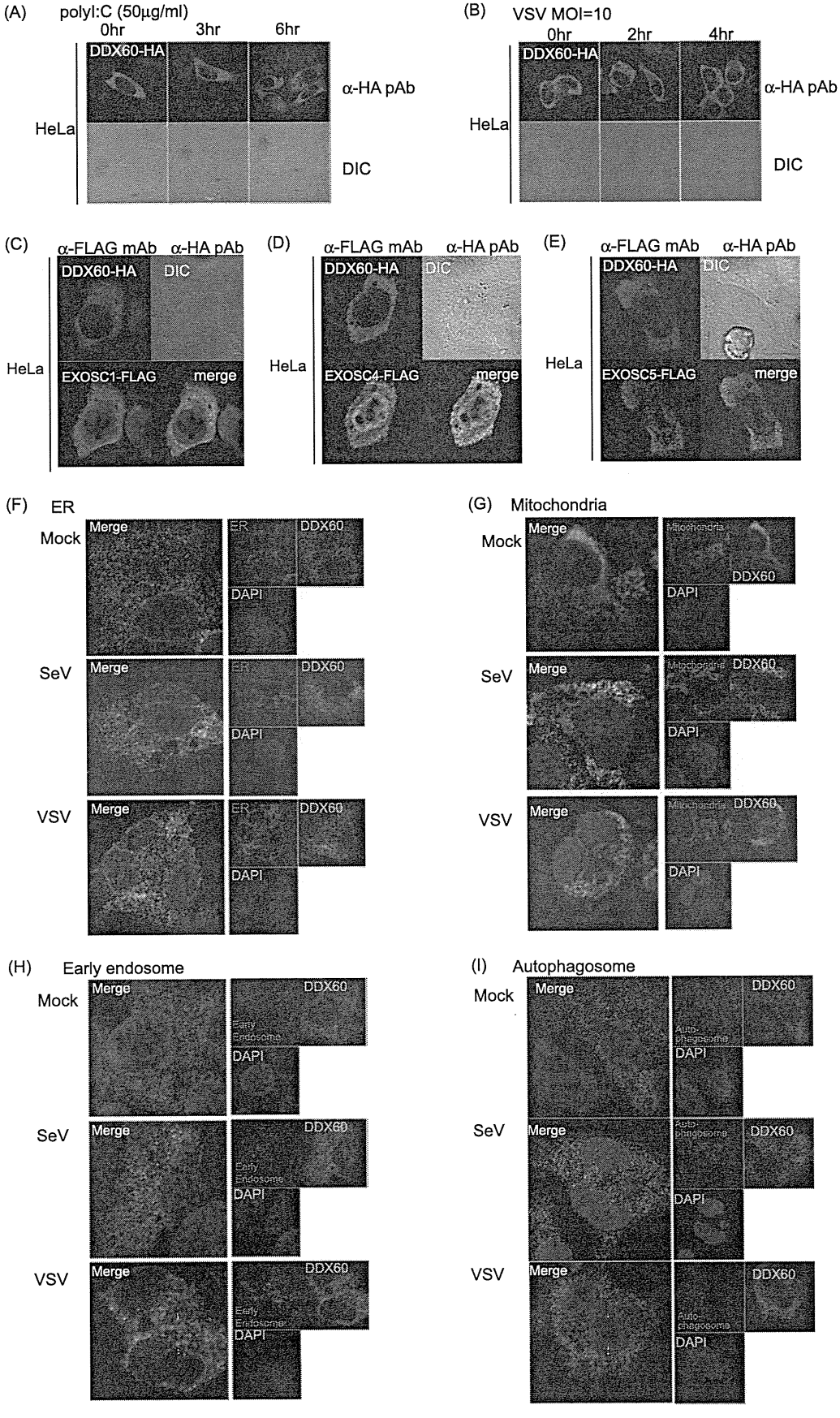
(A)
polyI:C (50μg/ml)
0hr
3hr
6hr
DDX60-HA
HeLa
α-HA pAb
DIC
(B)
VSV MOI=10
0hr
2hr
4hr
DDX60-HA
HeLa
α-HA pAb
DIC
(C)
α-FLAG mAb
α-HA pAb
DDX60-HA
DIC
HeLa
EXOSC1-FLAG
merge
(D)
α-FLAG mAb
α-HA pAb
DDX60-HA
DIC
HeLa
EXOSC4-FLAG
merge
(E)
α-FLAG mAb
α-HA pAb
DDX60-HA
DIC
HeLa
EXOSC5-FLAG
merge
(F)
ER
Mock
SeV
VSV
Merge
ER
DDX60
DAPI
(G)
Mitochondria
Mock
SeV
VSV
Merge
Mitochondria
DDX60
DAPI
(H)
Early endosome
Mock
SeV
VSV
Merge
DDX60
Early Endosome
DAPI
(I)
Autophagosome
Mock
SeV
VSV
Merge
DDX60
Auto-phagosome
DAPI

high-capacity cDNA reverse transcription kit (ABI). Quantitative PCR (qPCR) analysis was performed using Step One software version 2.0 (ABI) and SYBR Green Master Mix (ABI). The primer sequences for qPCR and PCR are described in Table S2 and S3 in the supplemental material, respectively.

Microarray analysis. Mouse bone marrow-derived dendritic cells were stimulated with poly(I · C) or infected with MV with anti-IFN-AR antibody (Ab) (see Fig. 2A). Total RNA was extracted from the cells, and we performed microarray analysis using Affimetrix GeneChip Mouse 430.2 software (10). The data were analyzed by GeneSpring GX 11 software.

RNA interference. RNA interference (RNAi) vectors were constructed by the insertion of oligonucleotides into the XbaI and PstI site of the pH 1 vector. The target sequence for DDX60 is 5′-CTTTACCACTTTCCTACGA-3′, the target sequence for EXOSC4 is 5′-TATAGTTCAGCGACCTT-3′, and the target sequence for EXOSC5 is 5′-GGATCCTACATCCAAGCAA-3′. HeLa cells or HEK293 cells were transfected with RNAi vector (0.5 μg) by the use of 24-well plates and FuGENE HD (Roche). After incubation for 24 h, cells were recovered and suspended in 12 ml of medium and then seeded to a 24-well plate. At 24 h after incubation, puromycin (1.0 μg/ml) was added. The medium containing puromycin was changed every 5 days, puromycin-resistant colonies were recovered, and the mRNAs of endogenous DDX60 or EXOSC4 and EXOSC5 were checked by RT-PCR. The sequences of the primers used for RT-PCR are described in Table S3 in the supplemental material. Small interfering RNA (siRNA) for DDX60 was purchased from Ambion and was transfected with Lipofectamine 2000 reagent (Invitrogen). The target sequence was 5′-GGC TAA CAA ACT TCG AAA A-3′.

Immunoprecipitation. HEK293FT cells were transfected in 6-well plates with plasmids encoding FLAG-tagged RIG-I, MDA5, EXOSC1, EXOSC4, EXOSC5, LGP2, IKK-ε, and Ubc13- and/or HA-tagged DDX60. The plasmid amounts were normalized by the addition of empty plasmid. At 24 h after transfection, cells were lysed with lysis buffer (20 mM Tris-HCl [pH 7.5], 150 mM NaCl, 1 mM EDTA, 10% glycerol, 1% Nonidet P-40, 30 mM NaF, 5 mM Na_3VO_4, 20 mM iodoacetamide, 2 mM phenylmethylsulfonyl fluoride), and then proteins were immunoprecipitated with rabbit anti-HA polyclonal antibody (Sigma) or anti-FLAG M2 monoclonal antibody (Sigma). The precipitates were analyzed by SDS-polyacrylamide gel electrophoresis (SDS-PAGE) and stained with anti-HA polyclonal or anti-FLAG M2 monoclonal antibody or monoclonal antibody to RIG-I (Alme-1) (Alexis Biochemicals).

Confocal microscopy. HeLa and HEK293 cells were plated onto Micro Cover glass sheets (Matsunami) and poly-L-lysin-coated cover glass sheets (eBioscience), respectively, in a 24-well plate. The following day, cells were transfected with the indicated plasmids. At 24 h after transfection, cells were infected with VSV or transfected with poly(I · C) by the use of 0.5 μg/ml DEAE-dextran for 4 h and then fixed using 3% formaldehyde–phosphate-buffered saline (PBS) for 30 min and permeabilized with 0.2% Triton X-100 for 15 min. Fixed cells were blocked in 1% bovine serum albumin (BSA)–PBS for 10 min and labeled with the indicated primary Abs (5 μg/ml) for 60 min at room temperature. Alexa-conjugated secondary Abs (1:400) were used to visualize staining of the primary Abs for 30 min at room temperature, and the mixture was mounted onto glass slides by the use of PBS containing 2.3% 1,4-diazabicyclo[2.2.2]octane and 50% glycerol or Prolong Gold antifade reagent with DAPI (4′,6′diamidino-2-phenylindole; Invitrogen). Cells were visualized at a magnification of ×63 with an LSM510 Meta microscope (Zeiss). To stain the mitochondria, endoplasmic reticulum (ER), early endosome, and autophagosome, we used Mitotracker (Invitrogen), anti-calnexin polyclonal antibody (Stressgen), anti-EEA1 polyclonal antibody (ABR), and anti-LC3 polyclonal antibody (MBL), respectively.

Reporter gene analysis. HEK293 cells were transiently transfected using 24-well plates and FuGENE HD (Roche) with expression vectors, reporter plasmids, and an internal control plasmid coding *Renilla* luciferase. The total amounts of plasmids were normalized with empty vector. For poly(I · C) stimulation, at 24 h after transfection, cells were stimulated with medium containing poly(I · C) (50 μg/ml) and DEAE-dextran (0.5 μg/ml) for 1 h, and then the medium was replaced with normal medium and incubation was performed for an additional 3 h. dsRNA was transfected using Lipofectamine 2000 (Invitrogen). Cells were lysed with lysis buffer (Promega) and luciferase, and *Renilla* luciferase activities were measured using a dual-luciferase assay kit (Promega). Relative luciferase activities were calculated by normalizing luciferase activity by control experiments in which only empty vector and reporter and internal control plasmids were transfected.

Viruses. VSV (Indiana strain), poliovirus (Mahoney strain), herpes simplex virus 1 (HSV-1) (K strain), and SeV (HVJ strain) were amplified using Vero cells. To determine the virus titer, we performed plaque assays using Vero cells. To observe the cytopathic effect (CPE), virus-infected cells were fixed at indicated times using 10% formaldehyde–PBS for 10 min and then stained using 1% crystal violet–PBS for 5 min at room temperature.

DDX60 helicase recombinant protein. The DDX60 helicase domain (bp 2254 to 4047) was amplified by PCR using primers DDX60 helicase-F and DDX60 helicase-R. The obtained cDNA fragment was cloned into KpnI and SalI restriction sites of pCold II DNA vector. The primer sequences were as follows: for DDX60 helicase-F, CGGGGTACCATGAGAAAAGACCCAG ATCCCAG; and for DDX60 helicase-R, GACGCGTCGACTTTTCCTATT TTGGGGAATG. The DDX6 helicase domain (aa 114 to 429) was amplified by RT-PCR using primers F (GGC GGG GTA CCA TGG GCT GGG AAA AGC CAT C) and R (GGA CGC GTC GAC ACC AAA GCG ACC TGA TCT TC). The cDNA fragment was cloned into the KpnI and SalI sites of pCold II DNA vector. Expression vectors were introduced into *Escherichia coli* BL21-competent cells and cultured in 10 ml of LB medium with ampicillin added for 12 h at 37°C and then added to 250 ml of LB medium and cultured for 3 h at 37°C. The cells were incubated at 15°C for 30 min, and protein expression was induced by the addition of 1 mM IPTG (isopropyl-β-D-thiogalactopyranoside). The cells were then cultured at 15°C for 24 h. The culture fluid was centrifuged for 10 min at 10,000 rpm and 4°C, and the *E. coli* cells were recovered. The cells were suspended in 5 ml of Tag binding buffer (20 mM Tris-HCl [pH 7.4], 0.5 M NaCl, 20 mM imidazol, 10% glycerol), 5 mg of lysozyme was added for 30 min on ice, and the mixture was subjected to shaking for 10 min; 500 μl of 10% Triton X-100 was then added, and the mixture was incubated for 10 min and centrifuged for 30 min at 5,000 rpm. The reaction was conducted at 4°C. The supernatant was subjected to filtration using a 0.45-μm-pore-size filter. The protein was purified using a HisTrap HP column (GE Healthcare) in accordance with the manufacturer's protocol. The protein was eluted with elution buffer (20 mM Tris-HCl [pH 7.4], 0.5 mM NaCl, 200 mM imidazol, 10% glycerol). We then collected the nonabsorbed fraction (that sample that had dropped out after the mixture was applied to the column), the wash fraction (the sample that dropped out after washing using the binding buffer was performed), and 500 μl each of elute fractions 1 to 10. The obtained samples were checked for purification by SDS-PAGE and detected by Coomassie brilliant blue (CBB) staining.

RNA synthesis. VSV-G RNA was synthesized from plasmids by using Riboprobe combination system SP6/T7 RNA polymerase (Promega) in accordance with the manufacturer's protocol. VSV RNA was produced from PCR products by the use of VSV G-pGEM-T Easy for its template and amplified by using a 5′ primer containing the T7 promoter (TAATACGACTCACTATAGGG) and a 3′ primer containing the SP6 promoter (GATTTAGGTGACACTATAG). The dsRNA was made by mixing equal amounts of positive strand (SP6) and negative strand (T7). The obtained ssRNA or dsRNA was added to 10 U of DNase I (Promega) at 37°C for 30 min and purified by phenol-chloroform treatment.

Gel shift assay. The components and final concentrations of the reaction solution were BSA (0.02 mg/ml), $MgCl_2$ (10 mM), dithiothreitol (DTT; 0.1 mM), glycerol (20%), NaCl (200 mM), Tris-HCl (20 mM), and ssRNA (0.6 μg), dsRNA (0.24 μg), or dsDNA (0.1 μg); we then added DDX60 or DDX6 helicase recombinant protein. The total volume was adjusted to 20 μl by adding water. The reaction solution was incubated at 30°C for 30 min; 1% agarose gel electrophoresis was then performed at 4°C for 90 min, and we observed the RNA results by the use of ethidium bromide (EtBr).

Pulldown assay. The RNA used for the assay was purchased from JBioS. The RNA sequences were as follows: for the sense strand, AAA CUG AAA GGG

FIG. 4. Intracellular localization of DDX60. (A and B) HA-tagged DDX60 expression vector was transfected into HeLa cells, and transfected cells were stimulated with 50 μg/ml poly(I · C) (A) or infected with VSV at an MOI of 10 (B). The cells were fixed and stained with anti-HA antibodies and observed using confocal microscopy. DIC, differential interference contrast; pAb, polyclonal antibody. (C to E) HA-tagged DDX60 was transfected into HeLa cells together with FLAG-tagged EXOSC1 (C), EXOSC4 (D), or EXOSC5 (E). Transfected cells were fixed and stained with anti-HA and anti-FLAG antibodies and observed using confocal microscopy. mAb, monoclonal antibody. (F to I) HEK293 cells stably expressing DDX60-HA were infected with VSV or SeV. DDX60-HA was stained with anti-HA antibody. The ER, mitochondria, early endosome, and autophagosome were stained with calnexin (F), Mitotracker Red (G), anti-EEA1 antibody (H), and anti-LC3 antibody (I).

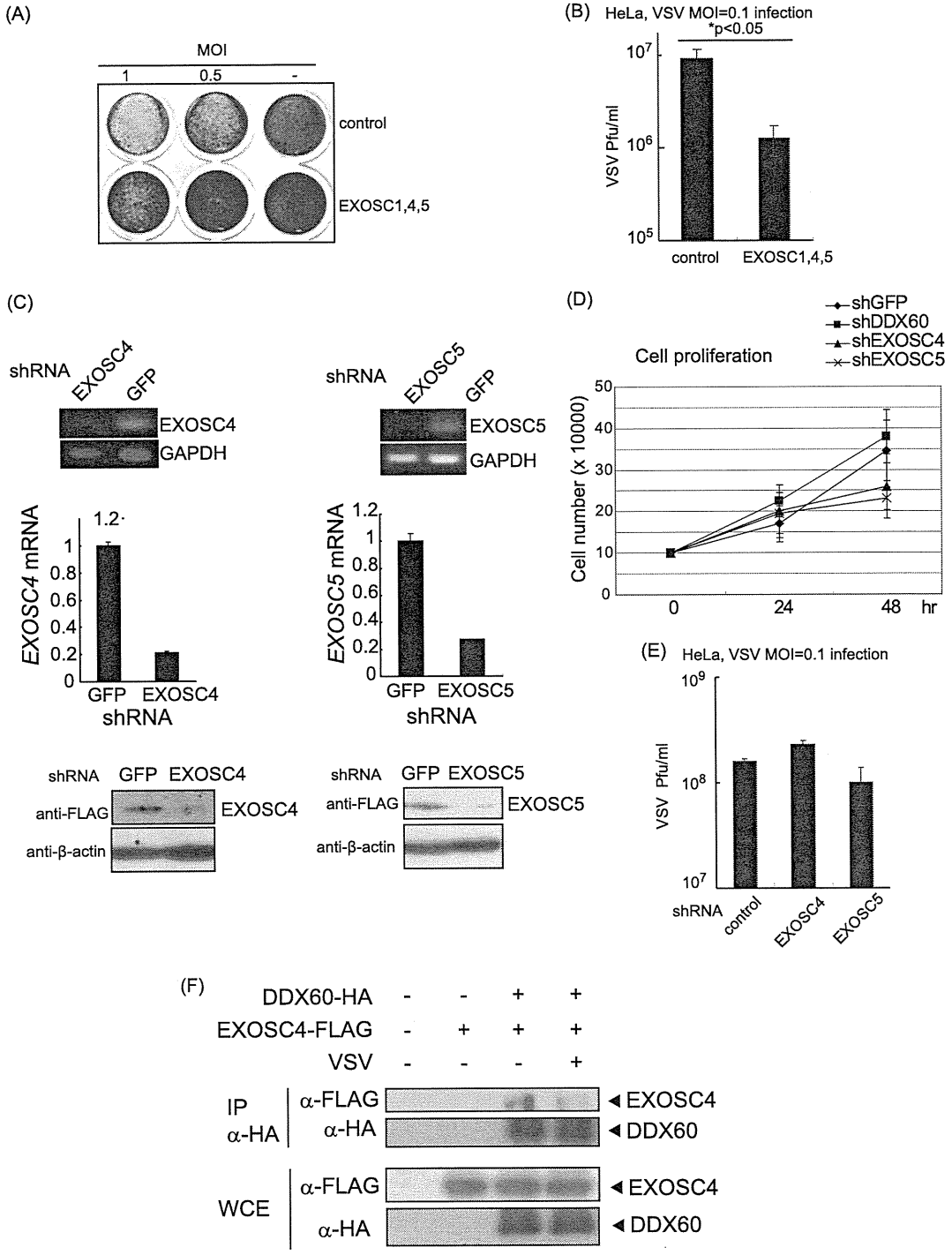

FIG. 5. Antiviral activity of RNA exosome. (A and B) HeLa cells were transfected with expression vectors containing EXOSC1, EXOSC4, and EXOSC5, and 24 h later, the transfected cells were infected with VSV at an MOI of 1 or 0.5. One day after infection, the cells were fixed and stained with crystal violet (A). Viral titers of culture media after 76 h were measured by a plaque assay (B). (C) Expression of EXOSC4 and EXOSC5 in stable HeLa clones, which express shRNA for EXOSC4, EXOSC5, or GFP, was examined by RT-PCR (upper panel), RT-qPCR (middle panel), and Western blotting (lower panel). The amounts of EXOSC4 and EXOSC5 cDNA in each sample were normalized by dividing by the amount of GAPDH. (D and E) Cell growth rates of stable HeLa clones, which express shRNA for EXOSC4, EXOSC5, DDX60, or GFP, were determined (D). The cells were infected with VSV at an MOI of 0.1 for 48 h, and viral titers of culture media were determined by a plaque assay (E). (F) FLAG-tagged EXOSC4- and HA-tagged DDX60-expressing vectors were transfected into HEK293FT cells. After VSV or mock infection, the immunoprecipitation was performed with anti-HA antibody.

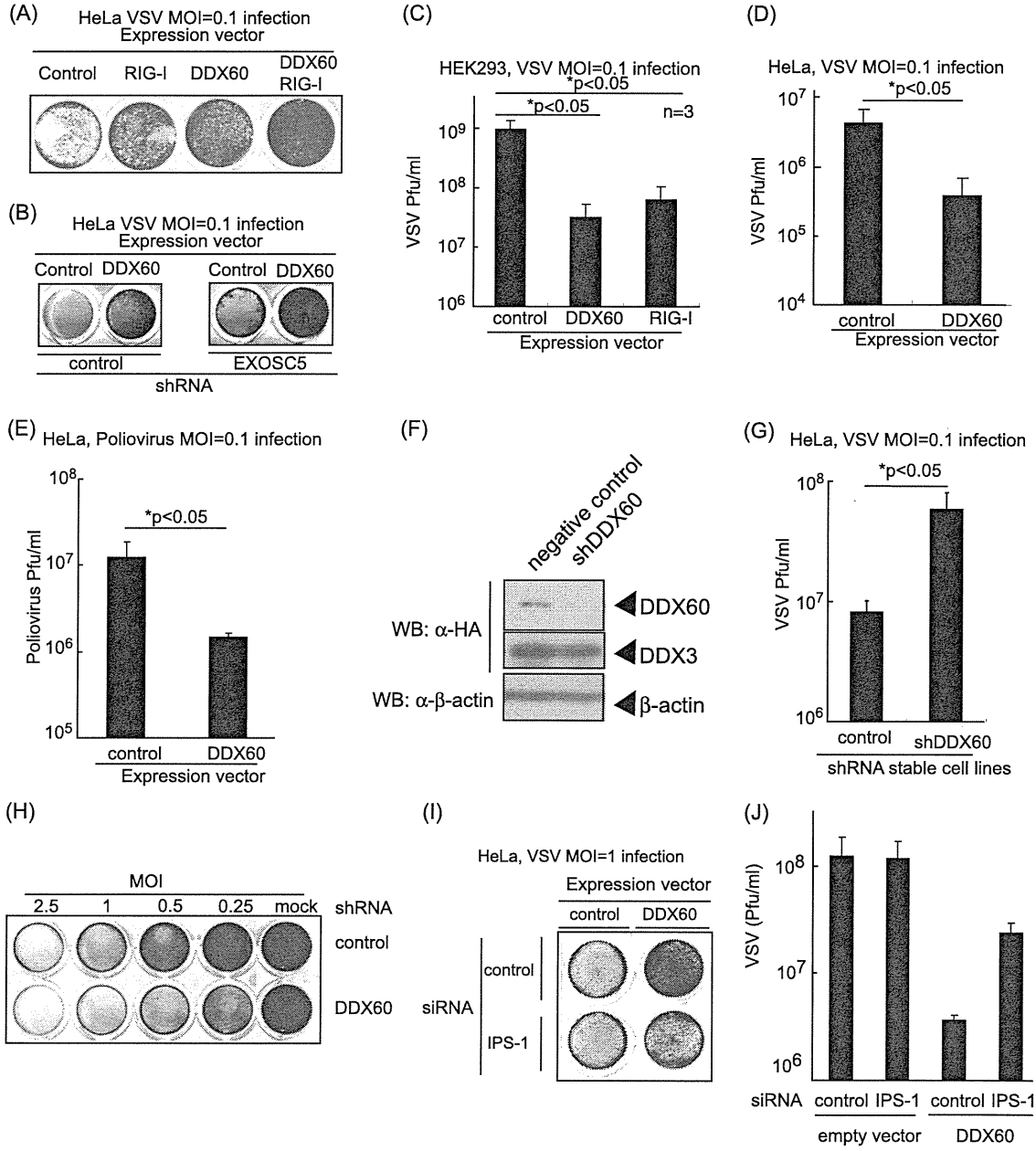

FIG. 6. Antiviral activity of DDX60. (A and B) HeLa cells (A) or the cells stably expressing shRNA for EXOSC5 or GFP (B) were transiently transfected with empty, DDX60-expressing, and/or RIG-I-expressing vectors. After 24 h, cells were infected with VSV at an MOI of 0.1 for 30 h. Cells were fixed and stained with crystal violet. (C and D) HEK293 clones stably expressing DDX60 or RIG-I (C) and HeLa cells subjected to mock treatment or transiently expressing DDX60 (D) were infected with VSV at an MOI of 0.1 for 24 h (C) or 48 h (D). Viral titers of culture media were measured by plaque assay. (E) Empty or DDX60-expressing vectors were transfected into HeLa cells, and 24 h after transfection, cells were infected with PV at an MOI of 0.1 for 26 h. Viral titers of culture media were measured by a plaque assay. (F) DDX60-expressing vector was transfected into HeLa clones stably expressing shRNA for GFP or DDX60, and the protein results were observed by Western blotting. (G) Control or DDX60 knockdown cells were infected with VSV at an MOI of 0.1 for 12 h, and viral titers of the culture media were measured by a plaque assay. (H) Control and DDX60 knockdown cells were infected with VSV at the indicated MOI for 12 h. The cells were fixed and stained with crystal violet. (I and J) Empty or DDX60-expressing vectors were transfected into HeLa cells with negative-control siRNA or siRNA for IPS-1. The cells were infected with VSV at an MOI of 1. After 24 h, cells were stained with crystal violet (I), and the viral titers of culture media were determined by a plaque assay (J).

AGA AGU GAA AGU G; and for the antisense strand, CAC UUU CAC UUC UCC CUU UCA GUU U. The biotin is conjugated at the U residue at the 3′ end of antisense strand (underlined). Biotinylated dsRNAs were phosphorylated by the use of T4 polynucleotide kinase (Takara). dsRNA was incubated for 1 h at 25°C with 10 μg of protein from the cytoplasmic fractions of cells that were transfected with FLAG-tagged RIG-I and/or HA-tagged DDX60-expressing vectors. The mixture was transferred into 400 μl of lysis buffer (20 mM Tris-HCl [pH 7.5], 150 mM NaCl, 1 mM EDTA, 10% glycerol, 1% NP-40, 30 mM NaF, 5 mM Na_3VO_4, 20 mM iodoacetamide, 2 mM phenylmethylsulfonyl fluoride [PMSF]) containing 25 μl of streptavidin Sepharose beads, rocked at 4°C for 2 h, collected by centrifugation, washed three times with lysis buffer, and resuspended in SDS sample buffer.

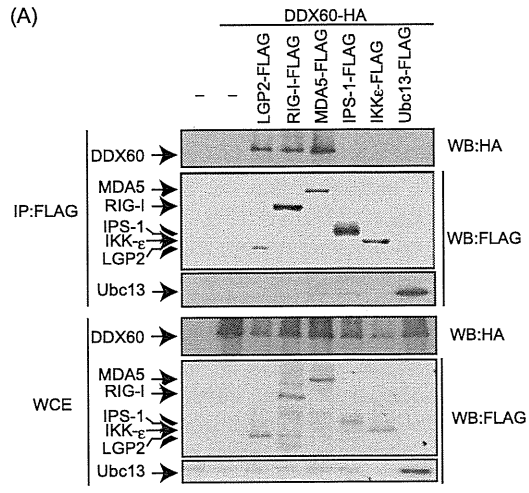
(A)
DDX60-HA
LGP2-FLAG
RIG-I-FLAG
MDA5-FLAG
IPS-1-FLAG
IKKε-FLAG
Ubc13-FLAG
IP:FLAG
WCE
DDX60
MDA5
RIG-I
IPS-1
IKK-ε
LGP2
Ubc13
WB:HA
WB:FLAG

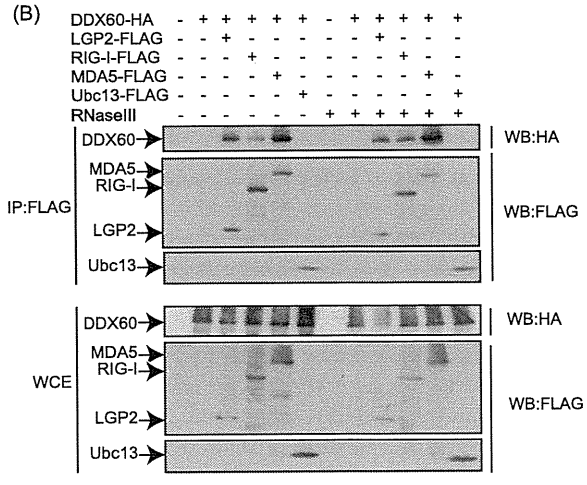
(B)
DDX60-HA
LGP2-FLAG
RIG-I-FLAG
MDA5-FLAG
Ubc13-FLAG
RNaseIII
IP:FLAG
WCE
DDX60
MDA5
RIG-I
LGP2
Ubc13
WB:HA
WB:FLAG

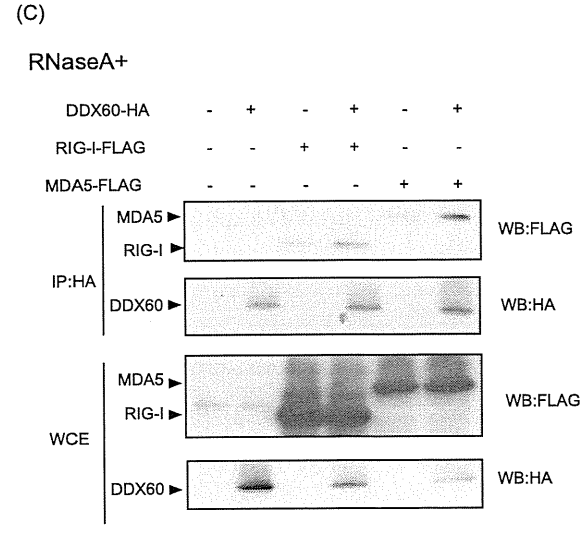
(C)
RNaseA+
DDX60-HA
RIG-I-FLAG
MDA5-FLAG
IP:HA
WCE
MDA5
RIG-I
DDX60
WB:FLAG
WB:HA

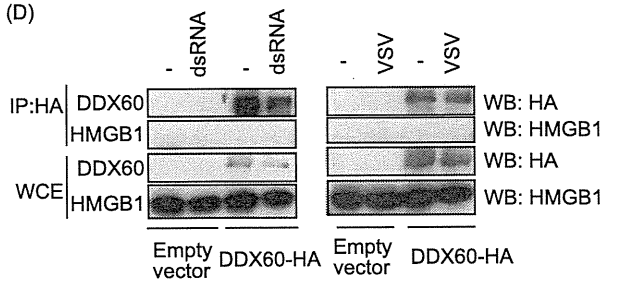
(D)
dsRNA
VSV
IP:HA
WCE
DDX60
HMGB1
WB: HA
WB: HMGB1
Empty vector
DDX60-HA

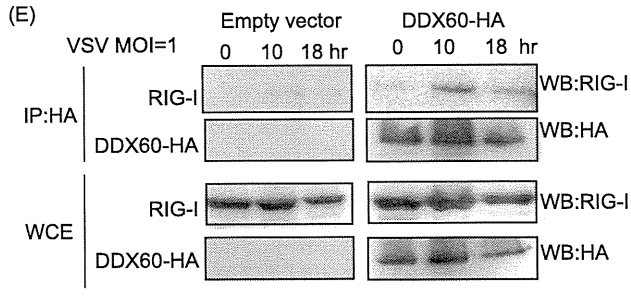
(E)
VSV MOI=1
Empty vector
DDX60-HA
0 10 18 hr
IP:HA
WCE
RIG-I
DDX60-HA
WB:RIG-I
WB:HA

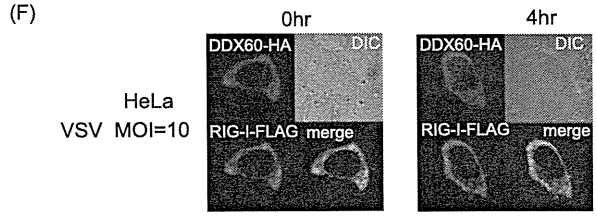
(F)
0hr
4hr
HeLa
VSV MOI=10
DDX60-HA
DIC
RIG-I-FLAG
merge

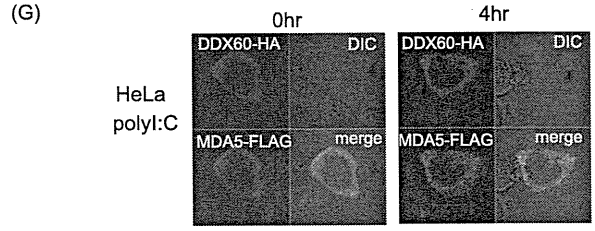
(G)
0hr
4hr
HeLa
polyI:C
DDX60-HA
DIC
MDA5-FLAG
merge

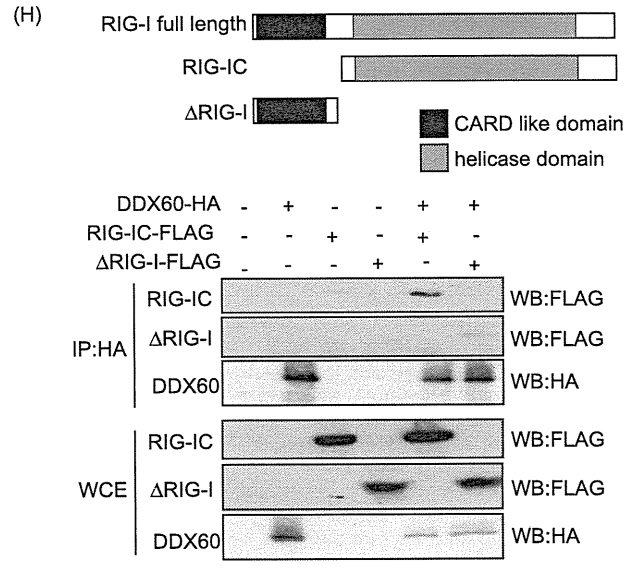
(H)
RIG-I full length
RIG-IC
ΔRIG-I
CARD like domain
helicase domain
DDX60-HA
RIG-IC-FLAG
ΔRIG-I-FLAG
IP:HA
WCE
DDX60
WB:FLAG
WB:HA

RESULTS

Phylogenetic analysis of the DEXD/H box domain of DDX60. The DDX60 protein contains a DEXD/H box RNA helicase domain and long N- and C-terminal regions with no typical domains or motifs (Fig. 1A). The DEXD/H box domain is common in the human genome. Phylogenetic analysis using amino acid sequences from this domain revealed that DDX60 is clustered within a group that includes RIG-I, MDA5, DICER1, and SKIV2L (bootstrap probability, 93%) and is most closely related to SKIV2L (bootstrap probability, 90%) (Fig. 1B). The functions of RIG-I and MDA5 have been described above. Dicer is an evolutionarily conserved protein required for RNAi and is known to perform antiviral functions in *Drosophila melanogaster* (12, 48, 51). SKIV2L is a homolog of *S. cerevisiae* Ski2, an antiviral protein that acts against dsRNA virus. Thus, the DDX60 DEXD/H box domain is found to cluster into a group composed of evolutionarily conserved antiviral helicases.

Expression of DDX60 mRNA. We carried out the microarray analysis using mouse bone marrow-derived dendritic cells (BM-DCs) and found that RLRs and DDX60 were included in the helicases whose expression had increased over 4-fold in response to viral infection (Fig. 2A and B). We investigated the expression profile of human DDX60 mRNA by Northern blot analysis and detected a single mRNA band at approximately 5.5 kb in the human brain, lymph node, prostate, stomach, thyroid, tongue, trachea, uterus, skeletal muscle, spleen, kidney, liver, and small intestine (Fig. 2C). Next, we examined the regulation of DDX60 expression. DDX60 mRNA was detected in unstimulated cells such as mouse BM-DCs, HeLa cells, HEK293 cells, and RAW 264.7 cells (Fig. 2D to F). DDX60 expression was upregulated by stimulation with poly(I · C) (Fig. 2D) or IFN-β (Fig. 2E). However, DDX60 expression was not increased by tumor necrosis factor alpha (TNF-α) or interleukin-1β (IL-1β) stimulation (Fig. 2E). Interestingly, DDX60 mRNA levels were increased by infection with VSV (Fig. 2F) or PV (Fig. 2G and H). Thus, DDX60 is an interferon-inducible gene and is upregulated during VSV or PV infection.

DDX60 associates with the components of the RNA exosome. Since the sequence of DDX60 is similar to that of RNA exosome cofactor SKIV2L, we examined whether the DDX60 protein associates with the RNA exosome core components in the same manner as the cofactor proteins. The RNA exosome core components form a tight protein complex (18); thus, it is expected that one of the core components would be coimmunoprecipitated with other core components and cofactors of the RNA exosome. These core components include EXOSC1 and EXOSC4. DDX60 protein was observed to coimmunoprecipitate with EXOSC1 and EXOSC4 (Fig. 3A and B), indicating the physical interaction of DDX60 with EXOSC1 and EXOSC4. We used partial DDX60 fragments to identify the region of DDX60 that binds to the RNA exosome. EXOSC4 was coimmunoprecipitated with the N-terminal 169-aa fragment of DDX60, indicating that the RNA exosome binds to the N-terminal region of DDX60 (Fig. 3C). All fragments were localized in the cytoplasmic region (Fig. 3D).

Intracellular localization of DDX60. Next, we studied the intracellular localization of the DDX60 protein by the use of confocal microscopy. In resting cells, DDX60 was localized in the cytoplasmic region but not in the nucleus before and after poly(I · C) stimulation or viral infection (Fig. 4A and B). EXOSC1, EXOSC4, and EXOSC5 were localized at both the cytoplasm and nucleus. The DDX60 protein was partially colocalized with the RNA exosome components at cytoplasmic region (Fig. 4C to E). To observe the intracellular localization of DDX60 after viral infection, we used HEK293 cell clones stably expressing HA-tagged DDX60. Most DDX60 staining was not colocalized with mitochondria, the endoplasmic reticulum (ER), LC3 (autophagosome marker), and endosome markers (EEA1) (Fig. 4F to I). However, the DDX60-HA protein was partially colocalized with the ER after VSV infection (Fig. 4F) and with the mitochondria after SeV infection (Fig. 4G).

Antiviral activity of DDX60 is independent of the RNA exosome. DDX60 expression was found to increase after viral infection, and the RNA exosome plays an antiviral role in lower eukaryotes such as budding yeast. Therefore, we assessed the antiviral activity of both DDX60 and the RNA exosome. Under our experimental conditions, 70% to 90% of cells expressed the proteins encoded by the transfected plasmids. Overexpression of three core components (EXOSC1, EXOSC4, and EXOSC5) suppressed the cytopathic effect (CPE) (Fig. 5A) and reduced the viral titer in the case of a low (0.1) multiplicity of infection (MOI) (Fig. 5B). Next, we performed a short hairpin RNA (shRNA) knockdown assay. We used shRNAs for EXOSC4 and EXOSC5, which were previously described as efficiently reducing expression of the target mRNA (4). We confirmed that shRNAs for EXOSC4 and EXOSC5 effectively reduced expression of their target mRNAs and the proteins (Fig. 5C). A partial decrease in levels of EXOSC4 in knockdown assays is known to reduce cell growth (47). We observed that the presence of shRNA for EXOSC4 and EXOSC5 reduced cell growth (Fig. 5D); how-

FIG. 7. Association of DDX60 with RLRs. (A to C) Vectors expressing HA-tagged DDX60 were transfected into HEK293FT cells with FLAG-tagged LGP2, RIG-I, MDA5, IPS-1, IKK-ε, and/or Ubc13, and cell lysates were prepared. The lysates were treated with RNase III (B) or RNase A (C). Immunoprecipitation was carried out with anti-FLAG antibody, and the precipitates (IP) and 10% of whole-cell extract (WCE) were analyzed using SDS-PAGE. Proteins were stained by Western blotting using anti-HA or anti-FLAG antibody. (D and E) HEK293FT cells were transfected with empty or HA-tagged DDX60-expressing vectors, and cells were stimulated with dsRNA or infected with VSV. Cell lysates were prepared at the indicated times, and immunoprecipitation was performed with anti-HA antibody. The precipitates were analyzed using SDS-PAGE, and Western blotting was carried out using anti-HA and anti-HMGB1 (D) or anti-RIG-I (E) antibodies. (F and G) Vectors expressing HA-tagged DDX60 and FLAG-tagged RIG-I (F) or MDA5 (G) were transfected into HeLa cells. After 24 h, cells were fixed and stained with anti-HA or anti-FLAG antibody and then observed using confocal microscopy. (H) The upper panel shows a schematic diagram of RIG-I partial fragments. The lower panel shows results of an immunoprecipitation assay performed as described for panel A. DDX60 was found to bind to the RIG-IC region.

ever, knockdown of EXOSC4 or EXOSC5 showed a marginal effect on VSV replication (Fig. 5E), at least under our experimental conditions. We do not exclude the possibility that knockdown of EXOSC4 or EXOSC5 is not an efficient method by which to reduce the antivirus role of the RNA exosome. Unexpectedly, the physical interaction between EXOSC4 and DDX60 was reduced after VSV infection (Fig. 5F).

We next examined the antiviral activity of DDX60. Interestingly, DDX60 overexpression suppressed the CPE induced by VSV infection and reduced VSV replication in HEK293 and HeLa cells (Fig. 6A to D). The suppression induced by DDX60 overexpression was observed even in EXOSC5 knockdown cells (Fig. 6B). PV replication was also suppressed by overexpression of DDX60 (Fig. 6E). Next, we performed a knockdown assay using shRNA for DDX60, which reduced expression of DDX60 mRNA and protein (Fig. 6F) (see also Fig. 11 and 12). Unlike the results seen with EXOSC4 and EXOSC5, knockdown of DDX60 increased VSV replication and enhanced CPE and did not inhibit cell growth (Fig. 5D and Fig. 6G and H). Because the interaction between DDX60 and the RNA exosome core component was reduced after viral infection, we examined the molecular mechanism by which DDX60 suppresses viral replication.

DDX60 associates with RIG-I-like receptors. To identify the antiviral pathway in which DDX60 is involved, we used immunoprecipitation assays to search for the protein that binds to DDX60. Because the RLR-dependent pathway plays an important role in the antiviral activity of the host cell, we examined the binding of DDX60 to proteins involved in this pathway. Interestingly, DDX60 was coimmunoprecipitated with RIG-I, MDA5, and LGP2 but not with IPS-1 or IKK-ε, which are downstream factors of RIG-I and MDA5 (Fig. 7A). RNase A or RNase III treatment did not abolish the interaction between DDX60 and RIG-I or MDA5 (Fig. 7B and C), indicating that these associations are not mediated via RNA. DDX60 did not bind to HMGB1 before or after dsRNA stimulation or VSV infection (Fig. 7D). To further confirm the binding of DDX60 to RIG-I, we examined the interaction of DDX60 with endogenous RIG-I by the use of anti-RIG-I monoclonal antibody. RIG-I mRNA levels are known to increase after viral infection (59). We observed an increase in RIG-I protein levels after poly(I · C) stimulation (data not shown). However, the protein level in HEK293FT cells was not increased after VSV infection in our experiment for unknown reasons (Fig. 7E). Endogenous RIG-I was found to interact with DDX60 after VSV infection but not in its absence (Fig. 7E), indicating that interaction between DDX60 and endogenous RIG-I is dependent on viral infection, although the interaction between overexpressed RIG-I and DDX60 was independent of viral infection.

Next, we used confocal microscopy to examine the intracellular colocalization of DDX60 with RIG-I and MDA5. Consistent with the immunoprecipitation assay, confocal microscopic analysis showed that DDX60 was partially colocalized with overexpressed RIG-I and MDA5 before and after VSV infection or poly(I · C) stimulation (Fig. 7F and G). We tried to observe endogenous RIG-I by confocal microscopy; however, we could not detect endogenous RIG-I in our tests for technical reasons. We also used RIG-I partial fragments to identify the region of RIG-I that binds to DDX60 (Fig. 7H). RIG-IC, which includes a helicase domain and CTD, was coimmunoprecipitated with DDX60, while the N-terminal CARD of RIG-I was not (Fig. 7H). These data indicate that DDX60 binds to the RIG-IC fragment.

The DDX60 helicase domain binds to viral RNA. In light of the binding of DDX60 to viral RNA sensors RIG-I and MDA5, we hypothesized that the RNA helicase domain of DDX60 binds to viral RNA. To test this hypothesis, we expressed a histidine-tagged DDX60 RNA helicase domain (aa 752 to 1337) in *E. coli* (Fig. 8A). The protein was purified using nickel-nitrilotriacetic acid (Ni-NTA) resin, analyzed by SDS-PAGE, and stained with CBB. Protein purity was found to be greater than 90% (Fig. 8B). VSV single- and double-stranded RNA was synthesized *in vitro*. Binding of the DDX60 helicase domain to *in vitro*-synthesized viral RNA was examined using gel-shift assays. Single- or double-stranded VSV RNA mobility was found to decrease as a result of the addition of DDX60 helicase (Fig. 8C and D). DDX60 was also found to bind to dsRNA treated with alkaline phosphatase, suggesting that the presence of 5′ triphosphate is nonessential for this binding (Fig. 8E). The mobility shift of ssRNA was different from that of dsRNA; this difference might have been a result of the stoichiometry assays. Interestingly, dsDNA was also shifted in the presence of DDX60 protein (Fig. 8F). As a control we used DDX6, a DEXD/H box RNA helicase distantly related to DDX60. DDX6 also bound to ssRNA (Fig. 8C); however, DDX6 only minimally reduced the mobility of dsRNA and dsDNA compared to DDX60 (Fig. 8D and F).

DDX60 promotes RIG-I- or MDA5-dependent expression of type I IFN. Next, we examined whether DDX60 is involved in RIG-I- or MDA5-mediated signaling. The prepared poly(I · C) solution contains various lengths of poly(I · C), both shorter and longer than 1 kbp (data not shown), in a mixture known to activate both RIG-I and MDA5 (20). Both RIG-I-mediated and MDA5-mediated IFN-β promoter activation by poly(I · C) transfection were enhanced by DDX60 expression (Fig. 9A and B). As a control we used DDX6, a helicase distantly related to DDX60. Expression of DDX6 produced neither a positive nor a negative effect on the RIG-I-dependent IFN-β promoter activation (Fig. 9C). To address the function of the DDX60 helicase domain, we introduced the mutation (K791A) on the Walker type ATP binding site, which is essential for ATPase activity of RNA helicase (50). The mutation reduced the enhancement of RIG-I-mediated IFN-β promoter activation by DDX60 (Fig. 9C). Knockdown analysis using shRNA for DDX60 showed that IFN-β promoter activation by viral dsRNA was reduced in DDX60 knockdown cells compared with control cells (Fig. 9D). To exclude the off-target effect, we also used siRNA for DDX60, whose target sequence is different from that of shRNA for DDX60. Expression of DDX60 was efficiently reduced by siRNA for DDX60, and the siRNA for DDX60 efficiently reduced IFN-β mRNA expression by poly(I · C) stimulation (Fig. 9E to G). These knockdown results are consistent with the overexpression results described above, providing further evidence that DDX60 promotes RLR-mediated IFN-β expression.

In contrast, TICAM-1- and TLR3-mediated IFN-β promoter activation was not increased by overexpression of DDX60 (Fig. 9H and I). In addition, poly(I · C) stimulation of TLR3 without transfection resulted in normal expression

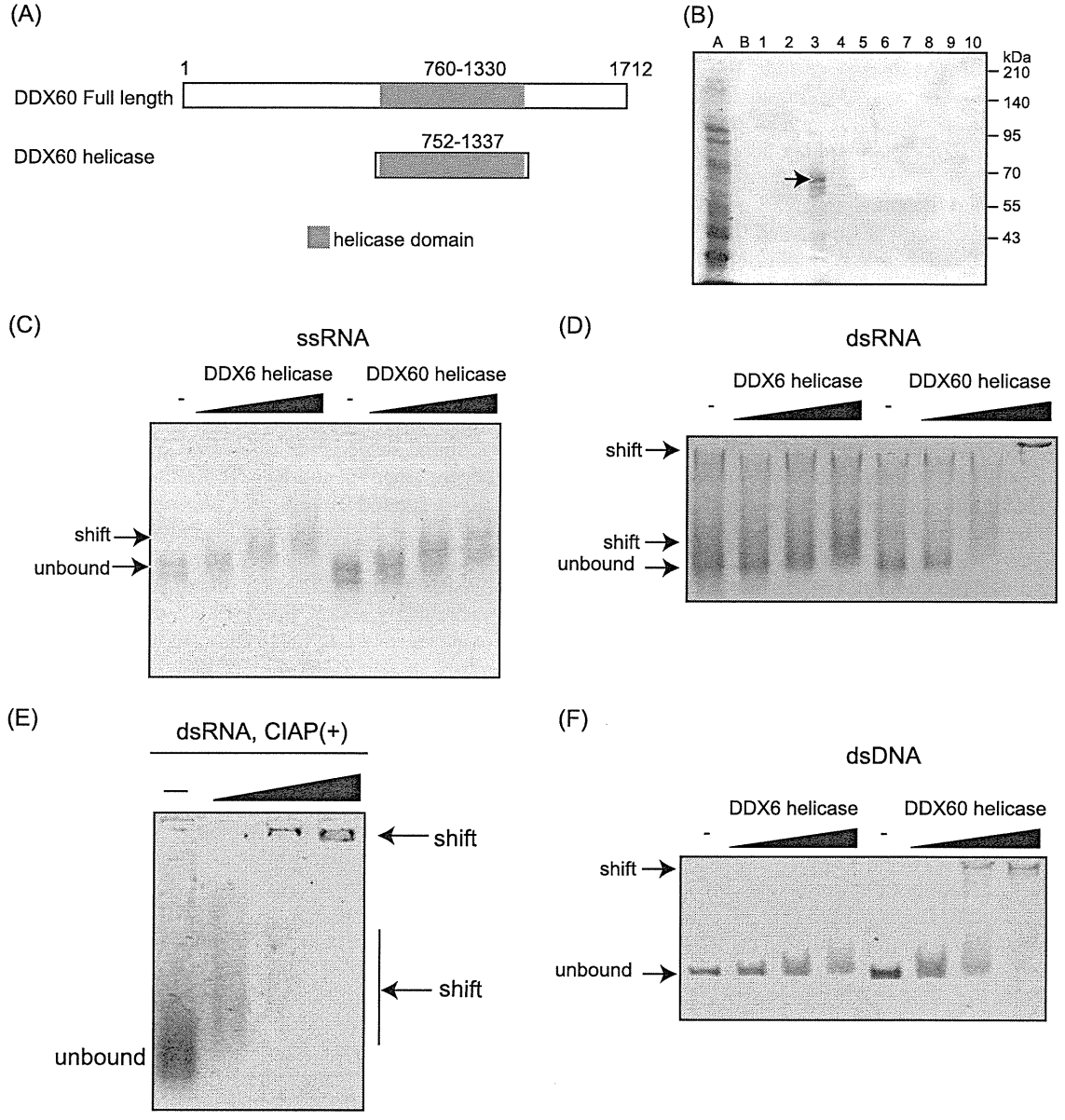

FIG. 8. Binding of the DDX60 helicase domain to viral RNA. (A) Schematic diagram showing the helicase region of DDX60 used for the following gel shift assay. (B) A His-tagged DDX60 helicase fragment was expressed in *E. coli* and purified using Ni-NTA resin. Purified products were analyzed by SDS-PAGE and stained with CBB. Lane A represents the nonabsorbed fraction, lane B represents the wash fraction, and lanes 1 to 10 represent the eluted fractions. The lane 3 fraction contains DDX60 protein. (C to F) Purified DDX60 and DDX6 fragments were incubated with *in vitro*-synthesized VSV ssRNA (C), dsRNA (D), dsRNA treated with calf intestinal alkaline phosphatase (CIAP) (E), or dsDNA (F), and the products were analyzed using agarose gel. The gel was stained with ethidium bromide.

of IFN-β in DDX60 knockdown cells (Fig. 9J). These data suggest that DDX60 is specific to the RLR pathway. Because the knockdown of EXOSC4 or EXOSC5 did not reduce the promoter activation resulting from VSV infection or dsRNA transfection (Fig. 9K and L), the data suggest that these proteins do not play a major role in DDX60-mediated enhancement of RIG-I or MDA5 signaling, at least under our experimental conditions. We also assessed the effect of DDX60 knockdown on IFN-β promoter activation by overexpressing TBK1, IPS-1, RIG-I CARDs, or MDA5 to discover the step at which DDX60 plays a role in RIG-I-mediated signaling. All of these procedures led to autoactivation, inducing transcription from the IFN-β promoter in the absence of RIG-I or MDA5 ligands (22). Although DDX60 knockdown reduces the IFN-β promoter activation induced by dsRNA transfection, it was not found to affect this autoactivation (Fig. 9M and N). These data suggest that shRNA suppression of DDX60 occurs upstream of RIG-I and MDA5 (Fig. 9O).

To examine the effect of DDX60 on the binding of RIG-I to dsRNA, we performed pulldown assays. The proteins were exogenously expressed in HEK293FT cells, and the proteins were recovered from cell lysates by the use of biotin-conjugated dsRNA and streptavidin Sepharose. RIG-I or DDX60 protein was recovered from cell extracts, suggesting the bind-

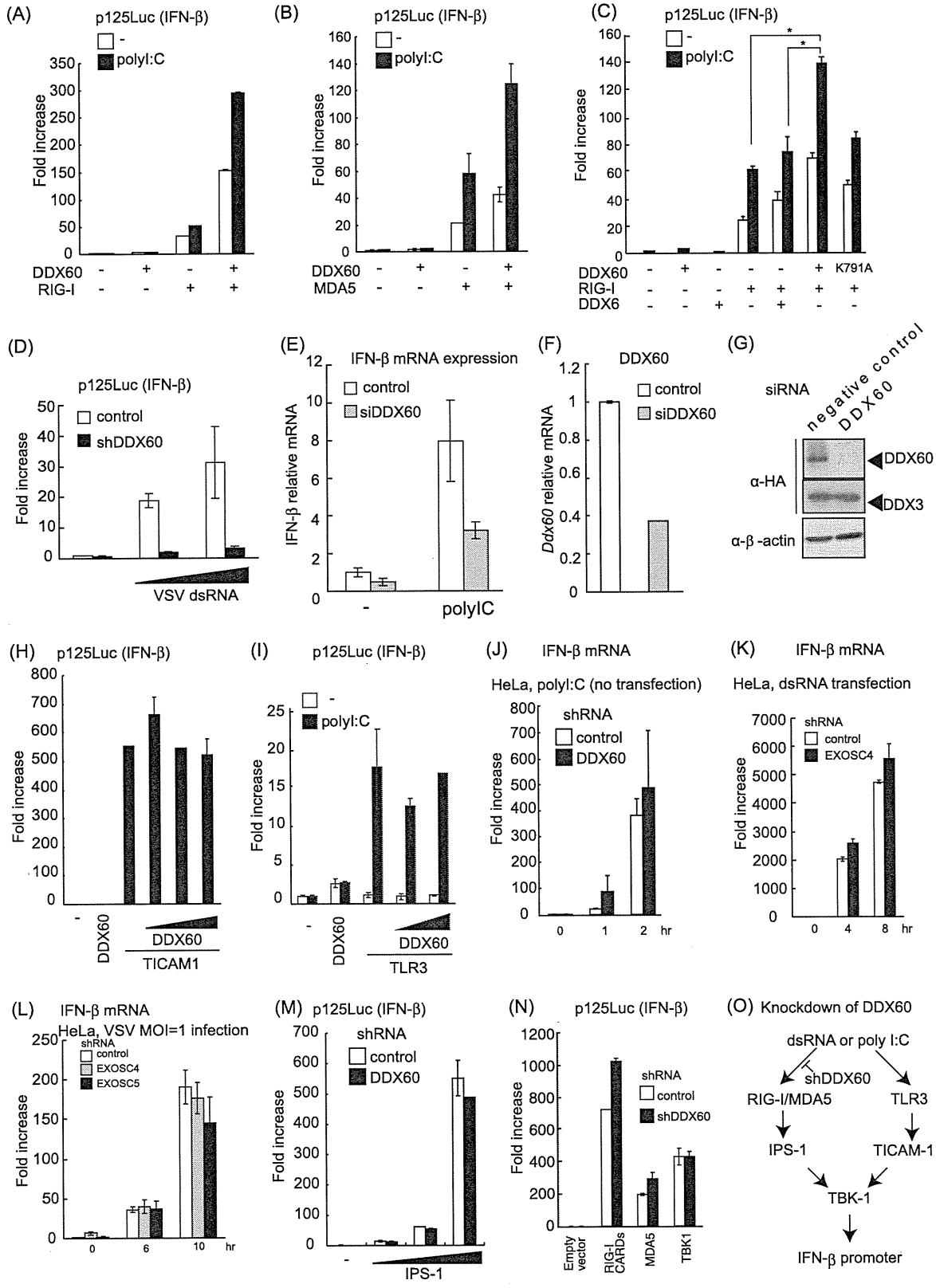

FIG. 9. DDX60 promotes RIG-I- or MDA5-mediated signaling. (A to C) Activation of the IFN-β promoter was examined using a reporter gene assay and p125luc plasmid. Vectors expressing RIG-I (A), MDA5 (B), DDX6 (C), and the wild type (WT) or DDX60-K791A (C) were transfected into HEK293 cells together with the reporter plasmid and *Renilla* luciferase plasmid (internal control). After 24 h, the cells were left unstimulated or stimulated with poly(I · C) by the use of DEAE-dextran for 4 h. Cell lysates were prepared, and luciferase activity was measured. (D) Control or DDX60 knockdown HEK293 cells were transfected with the p125luc reporter, *Renilla* luciferase plasmid, and/or *in vitro*-synthesized VSV